

An elastoplastic solution to undrained expansion of a cylindrical cavity in SANICLAY under plane stress condition

Authors: Lin. Li^{*a}, Haohua Chen^{b,c}, Jingpei Li^b, De'an Sun^d

First author: Dr. Lin Li

^aSchool of Highway, Chang'an University, Xi'an 710064, China

E-mail: lilin_sanmao@163.com

***Corresponding author: Ph. D. student Haohua Chen**

^bDepartment of Geotechnical Engineering, Tongji University; 1239 Siping Road, Shanghai, China.

^cDepartment of Civil and Architectural Engineering and Mechanics, The University of Arizona, Tucson, A.Z. 85721, U.S.A.

E-mail: howardchen@email.arizona.edu

Third author: Prof. Jingpei Li

^bDepartment of Geotechnical Engineering, Tongji University; 1239 Siping Road, Shanghai, China.

E-mail: lij2773@tongji.edu.cn

Fourth author: Prof. De'an Sun

^dDepartment of Civil Engineering, Shanghai University, Shanghai 200444, China.

E-mail: sundean06@163.com

1 **Abstract:** Although cylindrical cavity expansion under plane stress condition is commonly
2 encountered in geotechnical problems, most currently available solutions have been
3 developed for cavity expansion under plane strain condition. This paper develops a novel
4 elastoplastic solution for undrained expansion of a cylindrical cavity in SANICLAY under
5 plane stress condition. The SANICLAY model, which could well represent the mechanical
6 behaviour of the anisotropic soil and overconsolidated soil, is employed in the present
7 solution to model the responses of the soil around the expanding cavity. The problem is
8 formulated as a system of first-order differential equations with the unknown variables as
9 the function of an auxiliary coordinate, which are solved as an initial value problem. The
10 expansion responses under plane stress condition are comprehensively compared with
11 those under plane strain condition to highlight the unique expansion responses under plane
12 stress condition. The results show that the present solution could well reflect the unique
13 expansion responses under plane stress condition, which are totally different from those
14 under plane strain condition. It is expected the proposed solution could provide a
15 reasonable approach to interpret the pressuremeter test and model pile installation effects
16 near the surface of the natural anisotropic clays.

17 **Keywords:** plane stress condition; cross-anisotropy; undrained expansion; elastoplastic
18 solution; expansion responses

1. Introduction

Cavity expansion theory has a variety of applications in the analysis and design of many geotechnical problems (Yu, 2000; Mo and Yu 2018), such as interpretation of the in-situ cone penetration tests and pressuremeter tests (e.g., Wroth and Windle, 1975; Yu, 1990; Mayne, 1991; Burns and Mayne, 1998; Chang et al., 2001; Mo et al., 2016a; Suzuki and Lehane, 2015), modeling the pile installation effects (e.g., Randolph et al., 1979; Randolph 2003; Chai et al., 2005), prediction of the load carrying capacity of piles (e.g., Rezanian et al., 2017; Li et al., 2019, 2020), assessment of the stability of wellbore (e.g., Chen and Abousleiman, 2016; Zhou et al., 2021), as well as analysis of the excavation responses of tunneling (e.g., Yu and Rowe, 1999; Vrakas and Anagnostou, 2014, 2015, Mo and Yu, 2016b; Liang et al., 2016; Zou et al., 2019), etc.

Since Bishop et al. (1945) firstly developed a simple cavity expansion solution for metal indentation problems, much progress has been made to the cavity expansion theory and the cavity expansion theory gradually becomes a useful tool to solve a variety of geotechnical problems. The progress of cavity expansion theory in the past few decades can be broadly attributed to three aspects: 1) the development of new solution techniques for cavity expansion problem (e.g., Collins and Stimpson, 1994; Cao et al., 2001; Zhao, 2011; Chen and Abousleiman, 2012, 2013; Vrakas 2016); 2) analysis of cavity expansion responses in special soils, such as in the anisotropic soils (e.g., Li et al., 2016; Chen et al., 2019; Chen et al., 2020; Sivasithamparam and Castro, 2018, 2020; Chen and Liu, 2019), the unsaturated soils (e.g., Russell and Khalili, 2006; Chen et al., 2020; Yang et al. 2020),

and the thermoplastic soils (Zhou et al. 2018), etc.; 3) application of cavity expansion theory to solve the practical geotechnical problems (e.g., Mo et al., 2016; Mo and Yu, 2016; Li et al., 2017, 2019). Table 1 summarizes some recent representative solutions developed for cylindrical cavity expansion problems under different combinations of soil types, soil models and plane conditions. These research efforts, either development of the fundamental solution framework or application of the cavity expansion solution to geotechnical problems, have greatly improved and promoted the cavity expansion theory. However, almost all of the currently available solutions are developed for cavity expansion under plane strain conditions. Although the solutions under plane strain condition could properly interpret the pressuremeter tests and pile installation effects at a certain depth below the ground surface, the displacement of the soil near the ground surface is more similar to cavity expansion under plane stress condition. Recently, Su (2020) developed a rigorous elastoplastic solution for drained expansion of a cylindrical cavity under plane stress condition. Nevertheless, the undrained expansion of a cylindrical cavity under plane stress condition is still not yet available, especially when the anisotropic properties of the soil are involved. Therefore, it is of great significance to develop a rigorous elastoplastic solution for undrained expansion of a cylindrical cavity expansion under plane stress condition so as to better interpret the pressuremeter test and model pile installation effects in saturated clays near ground surface.

This paper presents a rigorous elastoplastic solution for undrained expansion of a cylindrical cavity in cross-anisotropic clays under plane stress condition. The advanced

SANICLAY model of Dafalias et al. (2006), which could properly model the mechanical behaviour of the anisotropic soils and the overconsolidated soils, is employed in the present solution to capture the expansion responses of the soil during cavity expansion. Taking advantage of the boundary condition, the plane stress condition, the undrained condition, the equilibrium equation and the elastoplastic constitutive relation of SANICLAY model, the cavity problem is formulated as a system of first-order differential equations as the governing equations. In the governing equations, all the unknown state variables that need to be determined are expressed as functions of an auxiliary coordinate, and thus the problem is readily solved as an initial value problem. Parametric studies are performed to investigate the undrained expansion responses under plane stress condition and the results from the present solution are comprehensively compared with those under plane strain condition to highlight the unique expansion responses under plane stress condition. It is expected that the proposed solution could better interpret and model pressuremeter tests and pile installation effects in saturated soil near the ground surface.

2. Definition of the problem

2.1 Plane stress condition

The plane stress condition for the undrained expansion of a cylindrical cavity is defined as the total vertical overburden pressure σ_z keeps constant during the cavity expansion process, which is commonly encountered in pressuremeter tests and pile installation within the area near the ground surface. Therefore, the plane stress condition

for the undrained expansion of a cylindrical cavity can be mathematically defined as

$$d\sigma_z = d\sigma'_z + du = 0 \quad (1)$$

where σ'_z denotes vertical effective stress; and u is the pore water pressure.

2.2 Description of the problem and basic assumptions

Fig. 1 schematically shows the undrained expansion of a cylindrical cavity under the plane stress condition. The soil mass is K_0 -consolidated with in-situ horizontal and vertical effective stresses σ'_{h0} and σ'_{v0} . The cavity expands from its initial cavity radius a_0 to the current cavity radius a under the internal cavity pressure σ_a . During this process, a plastic region with a radius of r_p is developed around the cavity wall, which is compassed by the outer elastic region. The soil mass near the cavity wall will be squeezed outwards and upwards under the internal cavity pressure. Note that the vertical strain, ε_z keeps zero under the plane strain condition during the cavity expansion process, while ε_z does not remain unchanged under the plane stress condition, which is the major difference between the two plane conditions. Although there will be both vertical and horizontal strains during cavity expansion, the problem considered is essentially one-dimensional as the cavity expands in a self-similar manner in the radial direction (Su 2020). Therefore, the equilibrium stress state of an arbitrary soil element around the cavity can be uniquely determined by the equilibrium equation in the radial direction alone, which gives

$$\frac{d\sigma'_r}{dr} + \frac{du}{dr} + \frac{\sigma'_r - \sigma'_\theta}{r} = 0 \quad (2)$$

The undrained expansion condition, which will be used to formulate the problem later

in the paper, means the volumetric strain ε_v of the soil around the cavity vanishes everywhere during the cavity expansion process, which gives

$$\varepsilon_v = -\ln\left(\frac{v}{v_0}\right) = 0 \quad (3)$$

where the logarithmic volume strain is employed in this study to accommodate the large strain in the plastic region during the cavity expansion process; v_0 and v are the initial specific volume and the current specific volume of the soil particle.

The underlying assumptions are made to develop the desired solution: 1) the compression stress and strain are taken as positive in this study, which is consistent with the traditional definition in soil mechanics; 2) the expansion is a relatively quick process and the coefficient of permeability of the clay is extremely small so that the expansion can be taken as an undrained process; 3) the K_0 -consolidated clay is vertical cross-anisotropy but transverse isotropy, and the axial of the cavity is perpendicular to the sediment plane; 4) the elastic behaviour is assumed to be isotropic and be represented by Hooke's law, whereas the plastic behaviour is anisotropic and can be properly modeled by the advanced SANICLAY model of Dafalias et al. (2006).

Based on the above definitions, the problem can be formulated in terms of the Lagrangian description with a proper constitutive model, as every soil particle around the cavity experiences the same stress and strain paths during cavity expansion due to the self-similar expansion manner.

2.3 SANICLAY model

In order to derive a general solution that is capable of reflecting the different expansion responses in soils with different overconsolidation ratios and degrees of anisotropy, the advanced SANICLAY model of Dafalias et al., (2006) is adopted in the present solution. The SANICLAY not only can properly represent initial stress anisotropy and stress-induced anisotropic behaviours of the K_0 consolidated clays, but also is capable of modeling both normally consolidated and overconsolidated soils as well as considering the three-dimensional strength of the soil. In light of these advantages, the SANICLAY model is selected in this study to derive a general solution for undrained expansion of a cylindrical cavity expansion under plane stress condition. The plastic potential function g of SANICLAY model in the general stress space is given as (Dafalias et al., 2006)

$$g = \frac{3}{2}(\mathbf{s} - p'\boldsymbol{\alpha}) : (\mathbf{s} - p'\boldsymbol{\alpha}) - \left(M^2 - \frac{3}{2}\boldsymbol{\alpha} : \boldsymbol{\alpha}\right)p'(p'_a - p') = 0 \quad (4)$$

where the symbol ‘:’ implies the trace of the product of two tensors; $\mathbf{s} = \boldsymbol{\sigma} - p'\mathbf{I}$ is the deviatoric stress tensor; p'_a is the value of p' at $q = p'\alpha$; q is the deviatoric stress; p' is the mean effective stress; \mathbf{I} is the identity tensor; $\boldsymbol{\alpha}$ is the non-dimensional anisotropic variable tensor, which serves as the rotational hardening parameters for the plastic potential yield function. M is the critical stress ratio. In SANICLAY model, M changes with Lode angle to represent the three-dimensional strength of the soil, which is defined as follows

$$M = \frac{2c}{(1+c)-(1-c)\cos 3\theta_L} M_c; \quad c = \frac{M_e}{M_c} \quad (5a)$$

$$\cos 3\theta_L = \sqrt{6}\text{tr } \mathbf{n}^3; \quad \mathbf{n} = \frac{\mathbf{r} - \boldsymbol{\alpha}}{[(\mathbf{r} - \boldsymbol{\alpha}) : (\mathbf{r} - \boldsymbol{\alpha})]^{1/2}}; \quad \mathbf{r} = \frac{\mathbf{s}}{p'} \quad (5b)$$

where M_c and M_e are the stress ratios at the critical state under the triaxial compression condition and extension condition, respectively.

In order to model the softening behaviour of K_0 consolidated clays under undrained loading, the non-associated flow rule is employed in SANICLAY model, which means the yield surface does not overlap the plastic potential surface. The yield function, f , of SANICLAY model in the general stress space is defined as (Dafalias et al., 2006)

$$f = \frac{3}{2}(\mathbf{s} - p'\boldsymbol{\beta}) : (\mathbf{s} - p'\boldsymbol{\beta}) - \left(N^2 - \frac{3}{2}\boldsymbol{\beta} : \boldsymbol{\beta}\right) p'(p'_c - p') = 0 \quad (6)$$

where $\boldsymbol{\beta}$ is the rotational hardening variable tensor of the yield surface. p'_c is the value of p' at $\eta = \beta$, which represents the isotropic hardening variable; N is a soil constant that is defined to model the peak strength and the softening behaviour after peak strength.

The hardening parameters of SANICLAY model, including the isotropic hardening parameter p'_c , the rotational hardening parameter tensors $\boldsymbol{\alpha}$ and $\boldsymbol{\beta}$, are defined in terms of the rate form as

$$\dot{p}'_c = \langle L \rangle \bar{p}'_c = \langle L \rangle \frac{v_0}{\lambda - \kappa} p'_c \operatorname{tr} \left(\frac{\partial g}{\partial \boldsymbol{\sigma}} \right) \quad (7)$$

$$\dot{\boldsymbol{\alpha}} = \langle L \rangle \bar{\boldsymbol{\alpha}} = \langle L \rangle \frac{v_0}{\lambda - \kappa} C \left(\frac{p'}{p'_c} \right)^2 \left| \operatorname{tr} \left(\frac{\partial g}{\partial \boldsymbol{\sigma}} \right) \right| \left[\frac{3}{2} (\mathbf{r} - \boldsymbol{\alpha}) : (\mathbf{r} - \boldsymbol{\alpha}) \right]^{1/2} (\boldsymbol{\alpha}^b - \boldsymbol{\alpha}) \quad (8a)$$

$$\boldsymbol{\alpha}^b = \sqrt{\frac{2}{3}} M \frac{(\mathbf{r}/x) - \boldsymbol{\alpha}}{[(\mathbf{r}/x - \boldsymbol{\alpha}) : (\mathbf{r}/x - \boldsymbol{\alpha})]^{1/2}} \quad (8b)$$

$$\dot{\boldsymbol{\beta}} = \langle L \rangle \bar{\boldsymbol{\beta}} = \langle L \rangle \frac{v_0}{\lambda - \kappa} C \left(\frac{p'}{p'_c} \right)^2 \left| \operatorname{tr} \left(\frac{\partial g}{\partial \boldsymbol{\sigma}} \right) \right| \left[\frac{3}{2} (\mathbf{r} - \boldsymbol{\beta}) : (\mathbf{r} - \boldsymbol{\beta}) \right]^{1/2} (\boldsymbol{\beta}^b - \boldsymbol{\beta}) \quad (9a)$$

$$\boldsymbol{\beta}^b = \sqrt{\frac{2}{3}} N \frac{\mathbf{r} - \boldsymbol{\beta}}{[(\mathbf{r} - \boldsymbol{\beta}) : (\mathbf{r} - \boldsymbol{\beta})]^{1/2}} \quad (9b)$$

where $\dot{}$ denotes the derivative of the variable; L is the loading index, which will be determined from the plastic consistency condition later in the paper. C is a model constant, which represents the rate of evolution of anisotropy; λ and κ are the slopes of normal compression and rebound lines, respectively; $\langle \rangle$ is the Macauley bracket to denote the events $\langle L \rangle = L$ when $L > 0$ and $\langle L \rangle = 0$ when $L \leq 0$.

The initial values of the non-dimensional anisotropic variable tensors α_{in} and β_{in} are related to the coefficient of lateral earth pressure at rest K_0 as follows

$$\alpha_{\text{in}} = \frac{\mathbf{r}_{\mathbf{k}0}}{x} = \frac{1}{x} \begin{bmatrix} \frac{K_0-1}{2K_0+1} & 0 & 0 \\ 0 & \frac{K_0-1}{2K_0+1} & 0 \\ 0 & 0 & \frac{2-2K_0}{2K_0+1} \end{bmatrix} \quad (10)$$

$$\beta_{\text{in}} = \mathbf{r}_{\mathbf{k}0} = \begin{bmatrix} \frac{K_0-1}{2K_0+1} & 0 & 0 \\ 0 & \frac{K_0-1}{2K_0+1} & 0 \\ 0 & 0 & \frac{2-2K_0}{2K_0+1} \end{bmatrix} \quad (11)$$

where x is a model parameter, which is introduced to control the saturation limit of anisotropy.

Fig. 2 schematically shows the geometries of the yield surface and plastic potential surface of SANICLAY model in $p' - q$ plane, and the model parameters defined in the model. It can be clearly seen that the yield surface is different from the plastic potential surface. The peak deviatoric stress q occurs on the yield surface at stress ratio N and is different from the deviatoric stress q at the final critical state, which allows for the modeling of softening behaviour after peak strength. Apart from the above-mentioned features, the SANICLAY model could also model other unique behaviours of soils, which, however, is beyond the scope of this study. One can refer to Dafalias et al. (2006) for more detailed information pertaining to the SANICLAY model.

3. Formulation of the problem

3.1 Constitutive matrix

Due to the symmetric nature of cylindrical cavity expansion problem, there will be only three principal stresses $\sigma'_r, \sigma'_\theta, \sigma'_z$ and the corresponding principal strains $\varepsilon_r, \varepsilon_\theta, \varepsilon_z$ involved, as the directions of the principal stresses entirely overlap the directions of the in-situ stresses of the K_0 consolidated cross-anisotropic soil. In the plastic region, the rate of the total strain consists of the elastic part and the plastic part, which gives,

$$\dot{\varepsilon}_r = \dot{\varepsilon}_r^e + \dot{\varepsilon}_r^p \quad (12a)$$

$$\dot{\varepsilon}_\theta = \dot{\varepsilon}_\theta^e + \dot{\varepsilon}_\theta^p \quad (12b)$$

$$\dot{\varepsilon}_z = \dot{\varepsilon}_z^e + \dot{\varepsilon}_z^p \quad (12c)$$

where $\varepsilon_r, \varepsilon_\theta, \varepsilon_z$ are the total strain in the radial, tangential and vertical directions. $\varepsilon_r^e, \varepsilon_\theta^e, \varepsilon_z^e$ and $\varepsilon_r^p, \varepsilon_\theta^p, \varepsilon_z^p$ are the elastic and plastic strains in the radial, tangential and vertical directions.

The rate of the elastic strain can be represented by Hooke's law as

$$\begin{bmatrix} \dot{\varepsilon}_r^e \\ \dot{\varepsilon}_\theta^e \\ \dot{\varepsilon}_z^e \end{bmatrix} = \frac{1}{E} \begin{bmatrix} 1 & -\nu' & -\nu' \\ -\nu' & 1 & -\nu' \\ -\nu' & -\nu' & 1 \end{bmatrix} \begin{bmatrix} \dot{\sigma}'_r \\ \dot{\sigma}'_\theta \\ \dot{\sigma}'_z \end{bmatrix} \quad (13)$$

where ν' is the effective Poisson's ratio; E is the elastic modulus, which depends on the current mean effective stress p' and the basic soil parameters as

$$E = \frac{3(1-2\nu')vp'}{\kappa} \quad (14)$$

Based on the plastic flow rule, the rate of the plastic strain can be written as

$$\dot{\varepsilon}^p = \langle L \rangle \frac{\partial g}{\partial \sigma} \quad (15)$$

where

$$\frac{\partial g}{\partial \sigma} = 3(\mathbf{s} - p'\boldsymbol{\alpha}) + \frac{1}{3}p'(M^2 - \eta^2)\mathbf{I} + \frac{\partial g}{\partial \theta_L} \frac{\partial \theta_L}{\partial \sigma} \quad (16a)$$

$$\frac{\partial g}{\partial \theta_L} = 6M^2 p' (p'_a - p') \frac{1-c}{(1+c)-(1-c) \cos 3\theta_L} \sin 3\theta_L \quad (16b)$$

$$\frac{\partial \theta_L}{\partial \boldsymbol{\sigma}} = -\frac{\sqrt{6}}{\sin 3\theta_L} \frac{\mathbf{n}^2 - \mathbf{n} \frac{\cos 3\theta_L}{\sqrt{6}} - \frac{1}{3} [1 + \text{tr}(\mathbf{n}^2 \boldsymbol{\alpha}) - \frac{\cos 3\theta_L}{\sqrt{6}} \text{tr}(\mathbf{n} \boldsymbol{\alpha})]}{[(\mathbf{s} - p' \boldsymbol{\alpha}) : (\mathbf{s} - p' \boldsymbol{\alpha})]^{1/2}} \quad (16c)$$

where $\eta = q/p'$ is the stress ratio.

The loading index L can be determined from the plastic consistency condition in the following. The plastic consistency condition gives

$$\dot{f} = \frac{\partial f}{\partial \boldsymbol{\sigma}} : \dot{\boldsymbol{\sigma}} + \frac{\partial f}{\partial \boldsymbol{\beta}} : \dot{\boldsymbol{\beta}} + \frac{\partial f}{\partial p'_c} \dot{p}'_c \quad (17)$$

Recalling Eqs. (7) and (9) that defines the rate of the hardening parameters \dot{p}'_c and $\dot{\boldsymbol{\beta}}$, and substituting them into Eq. (17), the loading index λ can be finally obtained as

$$\langle L \rangle = \frac{1}{K_p} \frac{\partial f}{\partial \boldsymbol{\sigma}} : \dot{\boldsymbol{\sigma}} \quad (18a)$$

$$K_p = -\left(\frac{\partial f}{\partial \boldsymbol{\beta}} : \dot{\boldsymbol{\beta}} + \frac{\partial f}{\partial p'_c} \dot{p}'_c \right) \quad (18b)$$

where

$$\frac{\partial f}{\partial p'_c} = -\left(N^2 - \frac{3}{2} \boldsymbol{\beta} : \boldsymbol{\beta} \right) p' \quad (19a)$$

$$\frac{\partial f}{\partial \boldsymbol{\beta}} = -3p'(\mathbf{s} - p'_c \boldsymbol{\beta}) \quad (19b)$$

$$\frac{\partial f}{\partial \boldsymbol{\sigma}} = 3(\mathbf{s} - p' \boldsymbol{\beta}) + \frac{1}{3} p' (N^2 - \eta^2) \mathbf{I} \quad (19c)$$

From Eq. (15), the rates of the three plastic strain components for cylindrical cavity expansion problem can be written in the matrix form as

$$\begin{bmatrix} \dot{\epsilon}_r^p \\ \dot{\epsilon}_\theta^p \\ \dot{\epsilon}_z^p \end{bmatrix} = \frac{1}{K_p} \begin{bmatrix} A_r B_r & A_r B_\theta & A_r B_z \\ A_\theta B_r & A_\theta B_\theta & A_\theta B_z \\ A_z B_r & A_z B_\theta & A_z B_z \end{bmatrix} \begin{bmatrix} \dot{\sigma}'_r \\ \dot{\sigma}'_\theta \\ \dot{\sigma}'_z \end{bmatrix} \quad (20)$$

where the matrix elements are given as

$$A_i = \frac{\partial g}{\partial \sigma'_i}; i = r, \theta, z \quad (21a)$$

$$B_i = \frac{\partial f}{\partial \sigma'_i}; i = r, \theta, z \quad (21b)$$

Combining Eqs. (12), (13) and (20) and taking inverse operation, the rates of stress components can be expressed in terms of the rates of the total strain components as follows

$$\begin{bmatrix} \dot{\sigma}'_r \\ \dot{\sigma}'_\theta \\ \dot{\sigma}'_z \end{bmatrix} = \frac{1}{H} \begin{bmatrix} H_r & H_{r\theta} & H_{rz} \\ H_{\theta r} & H_\theta & H_{\theta z} \\ H_{zr} & H_{z\theta} & H_z \end{bmatrix} \begin{bmatrix} \dot{\varepsilon}_r \\ \dot{\varepsilon}_\theta \\ \dot{\varepsilon}_z \end{bmatrix} \quad (22)$$

where the matrix elements are given as

$$H = (\nu' + 1) [K_p(1 - \nu' - 2\nu'^2) + E(1 - \nu')(A_r B_r + A_\theta B_\theta + A_z B_z) + E\nu'(A_r B_\theta + A_\theta B_r + A_\theta A_z + A_z A_\theta + A_z B_r + A_r b_z)] \quad (23a)$$

$$H_i = E [K_p(1 - \nu'^2) + E(A_j B_j + A_k B_k) + E\nu'(A_j B_k + A_j B_k)]; i, j, k = r, \theta, z; i \neq j \neq k \quad (23b)$$

$$H_{ij} = E [K_p(\nu' + \nu'^2) + E(A_k B_k - A_i B_j) - E\nu'(A_i B_k + A_k B_j)]; i, j, k = r, \theta, z; i \neq j \neq k \quad (23c)$$

It should be noted that the inverse operation intends to facilitate the formulation of the problem with the boundary condition and the undrained condition, which will be shown in detail in the following.

3.2 Governing differential equations

Firstly, an auxiliary variable ξ is defined in this study to reduce the unknown strain variables in the constitutive matrix so as to solve the problem considered. The idea of introducing an auxiliary variable to reduce the strain variables was firstly proposed by Chen and Abousleiman (2013) to formulate the drained expansion of a cavity under the plane

strain condition. However, the expression of the auxiliary variable ξ for cavity expansion under plane stress condition would be different from that under plane strain condition, as there will be vertical strain during cavity expansion. The auxiliary variable ξ in this study is defined as

$$\xi = \frac{U_r}{r} = \frac{r-r_0}{r} \quad (24)$$

where U_r denotes the radial displacement of a given soil particle located at radial location r ; r_0 is the initial radial location of the soil particle.

With the auxiliary variable defined by Eq. (24), the logarithmic radial strain ε_r and tangential strain ε_θ can be expressed as

$$\varepsilon_r = -\ln\left(\frac{dr}{dr_0}\right) = \ln\left(1 - \frac{dU_r}{dr}\right) = \ln\left(1 - \xi - r \frac{d\xi}{dr}\right) \quad (25a)$$

$$\varepsilon_\theta = -\ln\left(\frac{r}{r_0}\right) = \ln\left(1 - \frac{U_r}{r}\right) = \ln(1 - \xi) \quad (25b)$$

Making use of the undrained condition defined by Eq. (3) and Eqs. (25a) and (25b), the logarithmic tangential strain ε_r can be expressed by the tangential strain ε_θ and vertical strain ε_z as

$$\varepsilon_r = \varepsilon_v - \varepsilon_\theta - \varepsilon_z = -\ln(1 - \xi) - \varepsilon_z \quad (26)$$

From Eqs. (25a) and (26), the radial coordinate r can be related to the auxiliary variable ξ as

$$\frac{dr}{r} = \frac{d\xi}{1 - \xi - \frac{1}{(1-\xi)\exp(\varepsilon_z)}} \quad (27)$$

Now, the three unknown strain variables are essentially reduced to only one strain unknown variable ε_z by expressing the radial and tangential strains with the auxiliary variable and the vertical strain through Eqs. (25) and (26), which allows for the formulation

of the problem as differential equations in the following.

With the auxiliary variable, the constitutive relation of Eq. (22) can be expressed in terms of Lagrangian description as

$$\frac{D\sigma'_r}{D\xi} = \frac{1}{H} \left(H_r \frac{D\varepsilon_r}{D\xi} - H_{r\theta} \frac{1}{1-\xi} + H_{rz} \frac{D\varepsilon_z}{D\xi} \right) \quad (28a)$$

$$\frac{D\sigma'_\theta}{D\xi} = \frac{1}{H} \left(H_{\theta r} \frac{D\varepsilon_r}{D\xi} - H_\theta \frac{1}{1-\xi} + H_{\theta z} \frac{D\varepsilon_z}{D\xi} \right) \quad (28b)$$

$$\frac{D\sigma'_z}{D\xi} = \frac{1}{H} \left(H_{zr} \frac{D\varepsilon_r}{D\xi} - H_{z\theta} \frac{1}{1-\xi} + H_z \frac{D\varepsilon_z}{D\xi} \right) \quad (28c)$$

where the symbol 'D()' denotes differentials and derivatives of a given soil particle, i.e., the Lagrangian description.

On the other hand, the plane stress condition and the equilibrium equation should be combined with the constitutive functions Eq. (28) to formulate the problem considered. Introducing the auxiliary variable and the plane stress condition Eq. (1) into the equilibrium equation Eq. (2) gives

$$\left(\frac{D\sigma'_r}{D\xi} - \frac{D\sigma'_z}{D\xi} \right) \left[1 - \xi - \frac{1}{(1-\xi)\exp(\varepsilon_z)} \right] + \sigma'_r - \sigma'_\theta = 0 \quad (29)$$

Substituting Eqs. (28a) and (28c) into Eq. (29) gives

$$\frac{1}{H} \left[(H_r - H_{zr}) \frac{D\varepsilon_r}{D\xi} + (H_{r\theta} - H_{z\theta}) \frac{D\varepsilon_\theta}{D\xi} + (H_{rz} - H_{zz}) \frac{D\varepsilon_z}{D\xi} \right] \left[1 - \xi - \frac{1}{(1-\xi)\exp(\varepsilon_z)} \right] + \sigma'_r - \sigma'_\theta = 0 \quad (30)$$

Introducing the incremental form of undrained condition $D\varepsilon_r = -D\varepsilon_\theta - D\varepsilon_z$ into Eq. (30), the radial and vertical strain increments can be expressed with the stress components and the auxiliary variable as

$$\frac{D\varepsilon_r}{D\xi} = \frac{H}{H_{rz} - H_r - H_{zz} + H_{zr}} \frac{\sigma'_r - \sigma'_\theta}{1 - \xi - \frac{1}{(1-\xi)\exp(\varepsilon_z)}} - \frac{H_{r\theta} - H_{rz} - H_{z\theta} + H_{zz}}{H_{rz} - H_r - H_{zz} + H_{zr}} \frac{1}{1 - \xi} \quad (31a)$$

$$\frac{D\varepsilon_z}{D\xi} = \frac{H}{H_{rz}-H_r-H_{zz}+H_{zr}} \frac{\sigma'_r - \sigma'_\theta}{1 - \xi - \frac{1}{(1-\xi)\exp(\varepsilon_z)}} - \frac{H_{r\theta} - H_r - H_{z\theta} + H_{zr}}{H_{rz} - H_r - H_{zz} + H_{zr}} \frac{1}{1 - \xi} \quad (31b)$$

Note that Eqs. (31a) and (31b) are explicit functions of the unknown variables σ'_r , σ'_θ , σ'_z and ε_z , and hence Eqs. (28a)-(28c) should be the function of the unknown variables.

Considering the isotropic hardening parameter p'_c and the rotational hardening parameter tensors $\boldsymbol{\alpha}$ and $\boldsymbol{\beta}$ are given in the rate form, they should also be formulated as differential equations and solved together with Eqs. (28) and (31). Introducing the auxiliary variable to Eqs. (7), (8) and (9), the governing equations formulating the hardening parameters can be written as

$$\frac{Dp'_c}{D\xi} = \frac{1}{K_p} \frac{\partial f}{\partial \boldsymbol{\sigma}} : \frac{D\boldsymbol{\sigma}}{D\xi} \frac{v_0}{\lambda - \kappa} p'_c \operatorname{tr} \left(\frac{\partial g}{\partial \boldsymbol{\sigma}} \right) \quad (32a)$$

$$\frac{D\boldsymbol{\beta}}{D\xi} = \frac{1}{K_p} \frac{\partial f}{\partial \boldsymbol{\sigma}} : \frac{D\boldsymbol{\sigma}}{D\xi} \frac{v_0}{\lambda - \kappa} C \left(\frac{p'}{p'_0} \right)^2 \left| \operatorname{tr} \left(\frac{\partial g}{\partial \boldsymbol{\sigma}} \right) \right| \left[\frac{3}{2} (\mathbf{r} - \boldsymbol{\beta}) : (\mathbf{r} - \boldsymbol{\beta}) \right]^{1/2} (\boldsymbol{\beta}^b - \boldsymbol{\beta}) \quad (32b)$$

$$\frac{D\boldsymbol{\alpha}}{D\xi} = \frac{1}{K_p} \frac{\partial f}{\partial \boldsymbol{\sigma}} : \frac{D\boldsymbol{\sigma}}{D\xi} \frac{v_0}{\lambda - \kappa} C \left(\frac{p'}{p'_0} \right)^2 \left| \operatorname{tr} \left(\frac{\partial g}{\partial \boldsymbol{\sigma}} \right) \right| \left[\frac{3}{2} (\mathbf{r} - x\boldsymbol{\alpha}) : (\mathbf{r} - x\boldsymbol{\alpha}) \right]^{1/2} (\boldsymbol{\alpha}^b - \boldsymbol{\alpha}) \quad (32c)$$

Note that Eqs. (32a)-(32c), in terms of the tensor form, in fact correspond to seven differential equations, the detailed expressions of which are given in the appendix. Now Eqs. (28), (31b) and (32) formulate the problem considered as a system of eleven first-order differential equations, with the three stress components σ'_r , σ'_θ and σ'_z , the vertical strain ε_z , the isotropic hardening parameter p'_c and six anisotropic parameters $\alpha_r, \alpha_\theta, \alpha_z, \beta_r, \beta_\theta, \beta_z$ as the basic unknowns, which can be readily solved as an initial value problem if the initial values of these unknown variables are known. After determining these unknowns, the excess pore water pressures Δu can be obtained from the plane stress condition Eq. (1) as

$$\Delta u = u_0 - \sigma'_z + \sigma'_{v0} \quad (33)$$

It should be noted that since the governing equations are formulated with respect to the auxiliary coordinate ξ , the results solved from the governing equations are with respect to the auxiliary coordinate ξ rather than the real radial coordinate r . Therefore, the results should be related to the radial coordinate r by integrating Eq. (27) as

$$\frac{r}{a} = \exp\left(\int_{\xi_a}^{\xi} \frac{d\xi}{1-\xi-\frac{1}{(1-\xi)\exp(\epsilon_z)}}\right) \quad (34)$$

where $\xi_a (= 1 - a_0/a)$ represents the auxiliary coordinate at the cavity wall.

3.3 Initial conditions

The initial values of the rotational hardening parameter tensors $\boldsymbol{\alpha}_{\text{in}}$ and $\boldsymbol{\beta}_{\text{in}}$ have been already given by Eqs. (10) and (11), which can be determined from the coefficient of earth pressure at rest K_0 . The initial value of the isotropic hardening parameter $p'_{\text{c,in}}$ can be deduced from the overconsolidation ratio R as

$$p'_{\text{c,in}} = Rp'_0 \quad (35)$$

The initial values remaining to be determined are the values of the three stress components and the auxiliary variable at the instant that the soil particle turns into the plastic state, which can be determined by combining the yield function and the elastic solution. The elastic solution for cylindrical cavity expansion under plane stress condition should be identical to that under plane stress condition, as the excess pore water pressure, the vertical stress and the vertical strain keep unchanged in the elastic phase for both cases (Su 2020). The elastic solution for cylindrical cavity expansion problem has been well

developed by Yu (2000), which can be given as

$$\sigma'_r = \sigma'_{h0} - (\sigma'_{h0} - \sigma'_{rp}) \frac{r_p^2}{r^2} \quad (36a)$$

$$\sigma'_\theta = \sigma'_{h0} + (\sigma'_{h0} - \sigma'_{rp}) \frac{r_p^2}{r^2} \quad (36b)$$

$$\sigma'_z = \sigma'_{v0} \quad (36c)$$

$$U_r = -\frac{1+\nu'}{E} (\sigma'_{h0} - \sigma'_{rp}) \frac{r_p^2}{r} \quad (36d)$$

where σ'_{rp} denotes radial effective stress at the elastic-plastic boundary.

Combining Eqs. (6) and (36a)-(36c), σ'_{rp} can be obtained as

$$\sigma'_{rp} = K_0 \sigma'_{v0} + \frac{p'_0}{\sqrt{3}} \sqrt{\eta_p^{*2} - \eta_{in}^{*2}} \quad (37)$$

where p'_0 is the in situ values of the mean effective stress, η_{in}^* and η_p^* are given, respectively,

as

$$\eta_{in}^* = \sqrt{\frac{3}{2} (\mathbf{r}_{in} - \boldsymbol{\beta}_{in}) : (\mathbf{r}_{in} - \boldsymbol{\beta}_{in})} \quad (38a)$$

$$\eta_p^* = \sqrt{\left(N^2 - \frac{3}{2} \boldsymbol{\beta}_{in} : \boldsymbol{\beta}_{in}\right) \left[R \left(\frac{3 (\mathbf{r}_{in} - \boldsymbol{\beta}_{in}) : (\mathbf{r}_{in} - \boldsymbol{\beta}_{in})}{N^2 - \frac{3}{2} \boldsymbol{\beta}_{in} : \boldsymbol{\beta}_{in}} + 1 \right) - 1 \right]} \quad (38b)$$

in which

$$\mathbf{r}_{in} = \begin{bmatrix} \frac{\sigma'_{h0} - p'_0}{p'_0} & 0 & 0 \\ 0 & \frac{\sigma'_{h0} - p'_0}{p'_0} & 0 \\ 0 & 0 & \frac{\sigma'_{v0} - p'_0}{p'_0} \end{bmatrix} \quad (39)$$

Substituting Eqs. (37) into Eqs. (36a)-(36d) and noting the definition of the auxiliary variable, the initial values of the three stress variables $\sigma'_{r,in}$, $\sigma'_{\theta,in}$, $\sigma'_{z,in}$, the vertical strain $\varepsilon_{z,in}$, and the auxiliary coordinate ξ_{in}

$$\sigma'_{r,in} = \sigma'_{rp} = K_0 \sigma'_{v0} + \frac{p'_0}{\sqrt{3}} \sqrt{\eta_p^{*2} - \eta_{in}^{*2}} \quad (40a)$$

$$\sigma'_{\theta, \text{in}} = 2K_0\sigma'_{v0} - K_0\sigma'_{v0} - \frac{p'_0}{\sqrt{3}}\sqrt{\eta_p^{*2} - \eta_{\text{in}}^{*2}} \quad (40b)$$

$$\sigma'_{z, \text{in}} = \sigma'_{v0} \quad (40c)$$

$$\varepsilon_{z, \text{in}} = 0 \quad (40d)$$

$$\xi_{\text{in}} = \frac{\sigma'_{\text{rp}} - K_0\sigma'_{v0}}{2G} \quad (40e)$$

It can be seen that the initial values are independent of the radial location as the cavity expands in a self-similar manner, and hence the problem can be readily solved as an initial value problem with code developed by MATLAB solver.

4. Results and discussion

Extensive parametric studies, which cover a wide range of overconsolidation ratios, coefficients of earth pressure at rest, and specific volume to represent the different consolidation stress histories, are performed in this section to show the undrained expansion responses of a cylindrical cavity under plane stress condition. The soil parameters involved in the parameter analysis are summarized in table 2, in which most soil parameters are cited from Dafalias et al., (2006) while the parameters of soil with high overconsolidation ratios are extended by the authors with the aim to show the unique expansion responses in heavily overconsolidated soils. To highlight the differences between the expansion responses under plane stress and plane strain conditions, the results for plane strain condition will be also included in the following discussion for comparison.

4.1. Distributions of stress variables and anisotropic variables

Fig. 3 shows the distributions of the three stress components, the excess pore water pressure, the vertical strain and the distributions of the anisotropic variables in normally consolidated soils with $R = 1$ at the instant $a/a_0 = 1.018$ that the soil at the cavity wall reaches the critical state. The distributions of those variables under plane strain condition corresponding to $a/a_0 = 2$ are also included in Fig. 3(a) and 3(b) for comparison. In the figure, the stress components and the excess pore water pressure are normalized with respect to the in situ mean effective stress p'_0 and the radial coordinate is normalized with the instant cavity radius a . It should bear in mind that since the cavity expands in a self-similar manner, the distributions of the variables can be alternatively taken as the variations of the variables of a soil particle during cavity expansion.

As seen in Fig. 3a, the tangential and vertical stresses increase with the radial coordinate, while the radial stress increases then decreases with the radial coordinate in the normally consolidated soil. Given that the cavity expands in a self-similar manner, the above distribution curves indicate that the tangential and vertical stress components keep decreasing while the radial stress component increases and then decreases before the soil reaches the final critical state during the cavity expansion process. The tangential effective stress σ'_θ and the vertical effective stress σ'_z nearly approach the same value at the cavity wall, while the radial effective stress σ'_r is larger than σ'_θ and σ'_z , which indicates that the soil at the cavity wall tends to evolve from the initial vertical cross-anisotropy to the radial cross-anisotropy under the plane stress condition. However, although the soil around the cavity reaches the critical state under plane strain condition, the radial effective stress σ'_θ

and vertical effective stress σ'_z at the cavity wall do not approach the same value as the vertical deformation is restricted under plane strain condition. It is also interesting to see that the distributions of the stress components under plane stress condition are apparently different from those under plane strain condition. The three stress components keep unchanged around the cavity wall under the plane strain condition, while the stress components change significantly in the vicinity of the cavity wall under plane stress condition. This is because the vertical strain is restricted under the plane strain condition, and thus the stresses will keep constant values after the soil reaches the critical state. However, the vertical strain will develop indefinitely when the soil reaches the critical state under plane stress condition. As a consequence, the stresses will change significantly before the soil reaches the critical state under plane stress condition.

As seen in Fig. 3(b), negative vertical strain appears in the vicinity of the cavity, which means the soil around the cavity wall is severely pushed outwards in the vertical direction under the plane stress condition. This can well explain and model the ground surface heave phenomenon that is commonly encountered during pile installation. However, the vertical strain becomes negative and insignificant with the increase of the radial coordinate, which means the soil around the cavity firstly experiences a little inwards movement and then outwards movement in the vertical direction and the vertical strain primarily concentrates in the vicinity of the cavity wall for the normally consolidated soil. Positive excess pore water pressures are induced in the vicinity of the cavity wall under both plane strain and plane stress conditions. The positive excess pore water pressure decreases with the radial

coordinate, which means a hydraulic gradient forms in the radial direction during cavity expansion. Compared with the plane strain condition, the excess pore water pressure is more significant under the plane strain condition, since the deformation in the vertical direction is restricted under the plane strain condition.

From Fig. 3(c), it can be seen that the distributions of the anisotropic variables for potential surface α and for yield surface β show similar pattern, although the values of the anisotropic variable α are different from those of the anisotropic parameter β . It is interesting to note that the initial value of the anisotropic variable $\alpha_r(\beta_r)$ equals $\alpha_\theta(\beta_\theta)$ but is smaller than the anisotropic variable $\alpha_z(\beta_z)$, which reflects the vertical cross-anisotropy under initial K_0 -consolidated state. After cavity expansion, the anisotropic variables $\alpha_r(\beta_r)$ and $\alpha_z(\beta_z)$ nearly approach the same value at the cavity wall, while the anisotropic variable $\alpha_\theta(\beta_\theta)$ decreases from the initial value and is smaller than the values of $\alpha_r(\beta_r)$ and $\alpha_z(\beta_z)$ at the cavity wall.

Fig. 4 shows the distributions of the three stress components, the excess pore water pressure, the vertical strain and the distributions of the anisotropic variables in heavily overconsolidated soils with $R = 20$ at the instant $a/a_0 = 1.072$ that the soil at the cavity wall reaches the critical state. The distributions of those variables under plane strain condition with $a/a_0 = 2$ are also included in Fig. 4(a) and 4(b) for comparison. Again, the stress components and the excess pore water pressure are normalized with respect to the in situ mean effective stress p'_0 and the radial coordinate is normalized with the instant cavity radius a .

As seen in Fig. 4a, the distributions of the three stress components under plane stress condition are apparently different from those under plane strain condition, especially at the cavity wall. The radial and tangential effective stresses at the cavity wall under plane stress condition are higher than those under plane strain condition. The radial and tangential stresses under plane strain condition keep constant and reach the same value in the vicinity of the cavity, which means the soil around the cavity evolves from vertical cross-anisotropy to radial cross-anisotropy under the plane strain condition. However, this is not the case under the plane stress condition, since the values of the three stress components at the cavity wall are different from each other under plane stress condition. Moreover, it can be observed from Fig. 4(a) that there is an outer elastic zone around the cavity in the heavily overconsolidated soil, while the plastic region extends infinitely in the normally consolidated soil as observed in Fig. 3(a).

Significant different expansion responses of the excess pore water pressure can be observed from Fig. 4(b) under the plane strain and plane stress conditions. Negative excess pressure is developed around the cavity under plane stress condition, while positive excess pore water pressure is developed in the vicinity of the cavity wall under plane strain condition. This is because the soil potentially tends to dilatancy during cavity expansion, but the dilatancy is restricted under the plane strain condition. Therefore, the excess pore water pressure at the cavity wall firstly decreases to a negative value and then increases to a positive value under plane strain condition from the view of the self-similar expansion manner. Furthermore, the negative excess pore water pressure is a unique expansion

response in overconsolidated soil, as the positive excess pore water pressure is commonly developed in the normally and lightly overconsolidated soil, which will show in detail later in the paper. Corresponding to the excess pore water pressure, the vertical strain ε_z firstly are positive and then negative during the cavity expansion process, which indicates that the overconsolidated soil firstly develops inwards and then outwards displacement in the vertical direction during cavity expansion under plane stress condition from the self-similar expansion viewpoint.

From Fig. 4(c), it can be seen that the distributions of the anisotropic variable α and β again share similar patterns, although the values of α are different from the values of β . The initial value of $\alpha_r(\beta_r)$ equals $\alpha_\theta(\beta_\theta)$ but is larger than $\alpha_z(\beta_z)$ for the heavily overconsolidated vertical cross-anisotropic soil. After cavity expansion, the values of $\alpha_\theta(\beta_\theta)$ and $\alpha_z(\beta_z)$ tend to approach the same value although they finally do not reach the same value at the cavity wall under plane stress condition. This indicates that the soil at the cavity wall tends to but finally does not reach the radial cross-anisotropy under the plane stress condition for the heavily overconsolidated soil. In fact, the soil at the cavity wall also tends to but does not completely approach the radial cross anisotropy under plane strain condition (Sivasithamparam and Castro 2018), although the distributions of the anisotropic variables under plane strain condition are not shown in the figure.

To further explore the effects of the overconsolidation ratio R on the expansion responses, Figs. 5(a)-5(c) plot the distributions of the normalized radial effective stress, tangential effective stress, and vertical effective stress, respectively, under both plane stress

and strain conditions for different overconsolidation ratios. The radial coordinate is normalized with respect to the current cavity radius a again. It should be declared that the distributions of the stresses correspond to the instant that the soil at the cavity wall reaches the critical state for all the cases considered, and hence the final cavity radii are different for different R . The final cavity radii are $a/a_0 = 1.018, 1.015, 1.019, 1.044, 1.072$ for the cases of $R = 1, 5, 7, 10, 20$, respectively.

As seen from Fig. 5(a)-5(c), the radial effective stress σ'_r , the tangential effective stress σ'_θ and the vertical effective stress σ'_z at the cavity wall increase with the overconsolidation ratio under both plane stress and plane strain conditions for all the cases considered. This can be attributed to the fact that the potential strength and stiffness of the soil increase with the overconsolidation ratio. It is also interesting to note that the soil under plane stress condition approaches the critical state much more quickly than that under plane strain condition as no critical state region can be observed for the plane strain cases. This is because soil undergoes more severe shearing effects during cavity expansion under the plane strain condition. Another phenomenon that should be noted is that the three effective stresses at the cavity wall are larger than their initial values for all the cases considered except for the case $R = 1$, which indicates the expansion responses in overconsolidated soil are different from those in normally consolidated soil under plane stress condition. All the above observations demonstrate that the overconsolidation ratio has significant effects on the expansion responses under both plane stress and plane strain conditions.

Fig. 6 plots the distributions of the normalized excess pore water pressure at the instant

that the soil reaches critical state under plane stress condition for the cases of $R = 1, 5, 7, 10, 20$. The distributions of the normalized excess pore water pressure at the same cavity radius under plane strain condition are also included in the figure to highlight the different responses under plane strain and plane stress conditions. Again, the radial coordinate is normalized with respect to the current cavity radius a .

As seen in Fig. 6, since the overconsolidated soil tends to dilate while the normally consolidated soil tends to contract during cavity expansion under the plane stress condition, negative excess pore water pressures are developed in the vicinity of the cavity wall for all the cases considered, except for the case of $R = 1$. In contrast, positive excess pore water pressure is developed at the cavity wall under plane strain condition, although negative excess pore water pressure appears around the cavity. This is because the vertical strain is restricted under plane strain condition. As a consequence, the overconsolidated soil firstly tends to dilate and then contract during cavity expansion under the plane strain condition.

4.2 Expansion responses at cavity wall during expansion

Fig. 7 plots the expansion-pressure curves under both plane stress and plane strain conditions for the cases of $R = 1, 5, 7, 10, 20$. In the figure, the internal expansion pressure $\sigma_a (= \sigma'_r + \Delta u)$ is normalized with the initial mean effective stress p'_0 , and the cavity radius is normalized with respect to the initial cavity radius a_0 .

As seen in the figure, the internal expansion pressure increases with the expansion of the cavity under both plane stress and plane strain conditions. However, the expansion

pressure will not further develop when the soil reaches the critical state under plane stress condition, since the soil will deform indefinitely after reaching the critical state. In contrast, it is interesting to see that the expansion pressure still increases under the plane strain condition after the soil reaches the critical state, although the radial effective stress keeps constant, as shown in Fig. 5. In fact, the internal cavity pressure, i.e., the total radial stress, keeps increasing after the soil reaches the critical state until the cavity expands under an equilibrium state since a radial stress gradient is required to continuously push the soil outwards under plane strain condition. The expansion pressure also increases with the overconsolidation ratio, which indicates larger expansion pressure is required to expand the cavity in overconsolidated soils. It is also interesting to see that there is a discontinuous derivative point appearing in the expansion-pressure curve under plane stress condition, where the soil at the cavity wall reaches the plastic state. This is because vertical strain will develop under plane stress condition after the soil becomes the plastic state. In contrast, the expansion-pressure curve is smooth under the plane strain condition, as the strain of the soil is continuous under the plane strain condition.

Fig. 8 plots the variations of the excess pore water pressure at the cavity wall during cavity expansion under both plane stress and plane strain conditions for the cases of $R = 1, 5, 7, 10, 20$. In the figure, the excess pore water pressure is normalized with respect to the initial mean effective stress p'_0 and the current cavity radius is normalized with the initial cavity radius a_0 .

Inspection of Fig. 8 reveals that negative excess pore water pressure develops at the

cavity wall once the plastic deformation takes place state under plane stress condition except for the case of $R = 1$. The negative excess pore water pressure in overconsolidated soil increases with the expansion of the cavity and nearly approaches a constant value before the soil reaches the critical state under plane stress condition. In contrast, negative excess pore water pressure firstly develops at the cavity wall after the overconsolidated soil yielding under plane strain condition. With further expansion of the cavity, the excess pore water pressure increases and finally transforms to positive pressure under plane strain condition. As stated previously, the overconsolidated soil potentially tends to dilate under plane stress condition, while the tendency of dilatancy is restricted under plane strain condition. Therefore, negative excess pore water pressure develops at the cavity wall under plane stress condition. This is different from the plane strain condition with positive excess pore water pressure at the cavity wall. For the normally consolidated soil with $R = 1$, positive excess pore water pressure develops under both plane stress and plane strain conditions because the normally consolidated soil tends to contract during cavity expansion, which demonstrates the overconsolidation ratio has a significant effect on the excess pore water pressure developed during cavity expansion.

Fig. 9 plots the variation of the stress ratio with the deviatoric strain of the soil at the cavity wall under both plane stress and plane strain conditions so as to show the capability of the present solution in modeling the strain-softening behaviour of the soil during cavity expansion. Five different overconsolidation ratios, $R = 1, 5, 7, 10, 20$, are considered in the figure. As anticipated, the overconsolidated soil shows apparent strain-softening

behaviour, while the normally consolidated soil only shows strain-hardening behaviour under the plane stress condition. It can be seen that the peak stress ratio increases with the overconsolidation ratio, as the peak strength of the soil increases with the overconsolidation ratio. It is also interesting to note that, since the vertical strain is free of restriction under plane stress condition, the deviatoric strain required to mobilize the peak stress ratio under plane stress condition is smaller than that under plane strain condition for all the cases considered. Moreover, it can be observed that the final stress ratios at larger deviatoric strain are different from each other. This is because the strength of the soil depends on the effective stress state of the soil, which changes with Lode's angle as indicated by Eq. (5).

4.3 Effective stress path and evolutions of yield surface, potential surface

Fig. 10 and Fig. 11 plot the projections of the yield surface f , plastic potential surface g , the effective stress path (ESP) and the critical state line (CSL) in $p' - q$ plane and π plane for normally consolidated soil with $R = 1$ and heavily overconsolidated soil with $R = 20$, respectively. Only the curves under plane stress condition are plotted in the figure for clarity purposes.

As seen from Fig. 10(a), the initial effective stress point $(p'_0, \beta p'_0)$ is located at the intersection point of the β line and initial yield surface f and the initial plastic potential surface g passes through the initial effective stress point, which represents the initial stress state of the K_0 normally consolidated soil in the $p' - q$ plane. During the cavity expansion process, the ESP starts from the initial effective stress point and moves left to hit the CSL

line at the final critical state. Correspondingly, the yield surface f and plastic potential surface g contracts during the cavity expansion process, which indicates the soil undergoes isotropic volumetric softening. It is also interesting to see that the yield surface f and the plastic potential surface g rotate downwards in $p' - q$ plane, and rotate rightwards in π plane as shown in Fig. 10(b), which in fact show the evolution of the degree of anisotropy during cavity expansion. In π plane as shown in Fig. 10(b), the ESP starts from σ'_z axis, and moves right and downwards to touch the CSL in the vicinity of σ'_r axis.

As seen in Fig. 11, the ESP, the rotation of the yield and plastic potential surfaces of the overconsolidated soil are different from those of the normally consolidated soil in Fig. 10. It can be seen in Fig. 11(a) that the ESP of the overconsolidated soil starts from the initial stress point $(p'_0, \beta p'_0)$ that is located at the β line and within the yield and plastic potential loci. Since the mean effective stress keeps constant in the elastic expansion phase, the ESP moves vertically in the yield locus until touching the yield locus. After yielding, The ESP moves up and rightwards, which finally approaches the CSL when the soil reaches the critical state. Correspondingly, the plastic potential and yield loci enlarge and rotate upwards in $p' - q$ plane, which means the soil undergoes volumetric hardening and rotation hardening during the cavity expansion process. Correspondingly, in Fig. 11(b), it can be observed that the ESP starts from the initial stress point located at σ'_z axis, and moves horizontally right until touches the initial yield locus in π plane. After yielding, the ESP moves right and downwards to touch the CSL near the σ'_r axis in the π plane, which along with the evolutions of the yield and plastic potential loci again demonstrates the soil

tends to evolve from vertical cross-anisotropy to radial cross anisotropy during cavity expansion.

Apart from the above observations, it also interesting to see from Figs. 10(a) and 11(a) that the yield loci of the SANICLAY are circles in π plane, while the shape of plastic potential loci are similar to the shapes of SMP or Lade strength criterion in π plane. Hence, the three-dimensional strength of the soil is well represented by the plastic potential surface of SANICLAY model.

5. Summary and conclusions

This paper presents a rigorous elastoplastic solution to undrained expansion of a cylindrical cavity in SANICLAY under plane stress condition, which potentially could be applied to model the pressuremeter test and pile installation effects near the surface of the natural anisotropic clays. The advanced SANICLAY, which could properly model the strain-softening response under undrained loading, the initial stress anisotropy, stress-induced anisotropy of K_0 consolidated natural clays, the three-dimensional strength of the soil as well as the mechanical behaviours of overconsolidated soils, is employed in this study to derive a general solution for the problem considered. By subtly taking advantage of the equilibrium equation, the elastoplastic constitutive matrix, the undrained condition and the plane stress condition, the problem is formulated as a system of first-order differential equations in terms of Lagrangian description, which is readily solved as an initial value problem.

Extensive parametric analyses, which cover a wide range of soil parameters, are conducted to show the different expansion responses in soils with different consolidation stress histories. The results under plane stress condition are comprehensively compared with those under plane strain condition to highlight the effect of the plane stress condition. The results reveal that the expansion responses under plane stress condition are overall different from those under plane strain condition due to the different boundary conditions in the vertical direction. The different expansion responses include the distribution of the effective stress component, the development of the internal expansion pressure, the excess pore water pressures at the cavity wall and around the cavity, as well as the mobilization of the peak stress ratio. The most significant difference should be the negative excess pore water pressure is developed at the cavity wall in overconsolidated soils under plane stress condition. In contrast, the negative excess pore water pressure initially developed at the cavity wall finally decreases to positive excess pore water pressure with further expansion of the cavity under plane stress condition. Another difference worthy to note is that the strain of the soil at the cavity wall will develop indefinitely after the soil reaches the critical state under plane stress condition, while the cavity keeps expansion in a self-similar manner after the soil reaches the critical state under the plane strain condition. The results also indicate that the overconsolidated soil around the cavity evolves from the initial vertical cross-anisotropy to radial cross-anisotropy during the cavity expansion process. Moreover, the overconsolidation ratio has significant effects on the expansion responses under both plane stress and plane strain conditions.

Acknowledgements

The authors acknowledge the financial support provided by the National Natural Science Foundation of China (Grant No. 41772290).

Appendix. Detailed expressions of Eqs. (32a)-(32c)

Eqs. (32a)-(32c) are expressed in terms of tensor form, which in fact represent seven differential equations as shown in the following

$$\frac{Dp'_c}{D\xi} = \frac{1}{K_p} \left(\frac{\partial f}{\partial \sigma_r} \frac{D\sigma_r}{D\xi} + \frac{\partial f}{\partial \sigma_\theta} \frac{D\sigma_\theta}{D\xi} + \frac{\partial f}{\partial \sigma_z} \frac{D\sigma_z}{D\xi} \right) \frac{v_0}{\lambda - \kappa} p'_c \text{tr} \left(\frac{\partial g}{\partial \sigma} \right) \quad (\text{A1})$$

$$\frac{D\beta_r}{D\xi} = \frac{1}{K_p} \frac{\partial f}{\partial \sigma} : \frac{D\sigma}{D\xi} \frac{v_0}{\lambda - \kappa} C \left(\frac{p'}{p'_0} \right)^2 \left| \text{tr} \left(\frac{\partial g}{\partial \sigma} \right) \right| \left[\frac{3}{2} (\mathbf{r} - \boldsymbol{\beta}) : (\mathbf{r} - \boldsymbol{\beta}) \right]^{1/2} (\beta_r^b - \beta_r) \quad (\text{A2})$$

$$\frac{D\beta_\theta}{D\xi} = \frac{1}{K_p} \frac{\partial f}{\partial \sigma} : \frac{D\sigma}{D\xi} \frac{v_0}{\lambda - \kappa} C \left(\frac{p'}{p'_0} \right)^2 \left| \text{tr} \left(\frac{\partial g}{\partial \sigma} \right) \right| \left[\frac{3}{2} (\mathbf{r} - \boldsymbol{\beta}) : (\mathbf{r} - \boldsymbol{\beta}) \right]^{1/2} (\beta_\theta^b - \beta_\theta) \quad (\text{A3})$$

$$\frac{D\beta_z}{D\xi} = \frac{1}{K_p} \frac{\partial f}{\partial \sigma} : \frac{D\sigma}{D\xi} \frac{v_0}{\lambda - \kappa} C \left(\frac{p'}{p'_0} \right)^2 \left| \text{tr} \left(\frac{\partial g}{\partial \sigma} \right) \right| \left[\frac{3}{2} (\mathbf{r} - \boldsymbol{\beta}) : (\mathbf{r} - \boldsymbol{\beta}) \right]^{1/2} (\beta_z^b - \beta_z) \quad (\text{A4})$$

$$\frac{D\alpha_r}{D\xi} = \frac{1}{K_p} \frac{\partial f}{\partial \sigma} : \frac{D\sigma}{D\xi} \frac{v_0}{\lambda - \kappa} C \left(\frac{p'}{p'_0} \right)^2 \left| \text{tr} \left(\frac{\partial g}{\partial \sigma} \right) \right| \left[\frac{3}{2} (\mathbf{r} - x\boldsymbol{\alpha}) : (\mathbf{r} - x\boldsymbol{\alpha}) \right]^{1/2} (\alpha_r^b - \alpha_r) \quad (\text{A5})$$

$$\frac{D\alpha_\theta}{D\xi} = \frac{1}{K_p} \frac{\partial f}{\partial \sigma} : \frac{D\sigma}{D\xi} \frac{v_0}{\lambda - \kappa} C \left(\frac{p'}{p'_0} \right)^2 \left| \text{tr} \left(\frac{\partial g}{\partial \sigma} \right) \right| \left[\frac{3}{2} (\mathbf{r} - x\boldsymbol{\alpha}) : (\mathbf{r} - x\boldsymbol{\alpha}) \right]^{1/2} (\alpha_\theta^b - \alpha_\theta) \quad (\text{A6})$$

$$\frac{D\alpha_z}{D\xi} = \frac{1}{K_p} \frac{\partial f}{\partial \sigma} : \frac{D\sigma}{D\xi} \frac{v_0}{\lambda - \kappa} C \left(\frac{p'}{p'_0} \right)^2 \left| \text{tr} \left(\frac{\partial g}{\partial \sigma} \right) \right| \left[\frac{3}{2} (\mathbf{r} - x\boldsymbol{\alpha}) : (\mathbf{r} - x\boldsymbol{\alpha}) \right]^{1/2} (\alpha_z^b - \alpha_z) \quad (\text{A7})$$

where

$$\frac{\partial f}{\partial \sigma} : \frac{D\sigma}{D\xi} = \frac{\partial f}{\partial \sigma_r} \frac{D\sigma_r}{D\xi} + \frac{\partial f}{\partial \sigma_\theta} \frac{D\sigma_\theta}{D\xi} + \frac{\partial f}{\partial \sigma_z} \frac{D\sigma_z}{D\xi} \quad (\text{A8})$$

$$\text{tr} \left(\frac{\partial g}{\partial \sigma} \right) = \left(\frac{\partial g}{\partial \sigma_r} + \frac{\partial g}{\partial \sigma_\theta} + \frac{\partial g}{\partial \sigma_z} \right) \quad (\text{A9})$$

$$(\mathbf{r} - \boldsymbol{\beta}) : (\mathbf{r} - \boldsymbol{\beta}) = (r_r - \beta_r)^2 + (r_\theta - \beta_\theta)^2 + (r_z - \beta_z)^2 \quad (\text{A10})$$

$$(\mathbf{r} - x\boldsymbol{\alpha}) : (\mathbf{r} - x\boldsymbol{\alpha}) = (r_r - x\alpha_r)^2 + (r_\theta - x\alpha_\theta)^2 + (r_z - x\alpha_z)^2 \quad (\text{A11})$$

References

- Bishop, R.F., Hill, R., Mott, N.F., 1945. Theory of indentation and hardness tests. *Proc. Phys. Soc.* 57, 1477-159.
- Burns, S.E., Mayne, P.W., 1998. Monotonic and dilatatory pore-pressure decay during piezocone tests in clay. *Can. Geotech. J.* 35(6), 1063–1073.
- Cao, L.F., Teh, C.I., Chang, M.F. 2001. Undrained cavity expansion in modified Cam clay I: theoretical analysis. *Géotechnique* 51(4), 323–334.
- Chai, J., Miura, N., Koga, H., 2005. Lateral Displacement of Ground Caused by Soil–Cement Column Installation. *J. Geotech. Geoenviron. Eng.* 131(5), 623–632.
- Chang, M.F., Teh, C.I., Cao, L.F., 2001. Undrained cavity expansion in modified Cam Clay II: Application to the interpretation of the piezocone test. *Géotechnique* 51(4), 335–350.
- Chen, H.H., Li, L., Li, J.P., 2019. Stress transform method to undrained and drained expansion of a cylindrical cavity in anisotropic modified cam-clay soils. *Comput. Geotech.* 106, 128–142.
- Chen, H.H., Li, L., Li, J.P., Sun, D.A., 2020. Elastoplastic solution to drained expansion of a cylindrical cavity in anisotropic critical-state soils. *J. Eng. Mech.* 146(5), 04020036. 1–12.
- Chen, H.H., Li, L., Li, J.P., Sun, D.A., 2020. Elastoplastic solutions for cylindrical cavity expansion in unsaturated soils. *Comput. Geotech.* 123, 103569.

- Chen, S.L., Abousleiman, Y.N. 2016. Drained and undrained analyses of cylindrical cavity contractions by bounding surface plasticity. *Can. Geotech. J.* 53(9), 1398–1411.
- Chen, S.L., Abousleiman, Y.N., 2012. Exact undrained elasto-plastic solution for cylindrical cavity expansion in modified Cam Clay soil. *Géotechnique* 62(5), 447–56.
- Chen, S.L., Abousleiman, Y.N., 2013. Exact drained solution for cylindrical cavity expansion in modified Cam Clay soil. *Géotechnique* 63(6), 510–517.
- Chen, S.L., Liu, K., 2019. Undrained cylindrical cavity expansion in anisotropic critical state soils. *Géotechnique* 63(6), 510–517.
- Collins, I.F., Stimpson, J.R. 1994. Similarity solutions for drained and undrained cavity expansions in soils. *Géotechnique* 44(1), 21–34.
- Dafalias, Y.F., Manzari, M.T., Papadimitriou, A.G., 2006. SANICLAY: simple anisotropic clay plasticity model. *Int. J. Numer. Anal. Meth. Geomech.* 30(12), 1231–1257.
- Li, L., Chen, S.L., Zhang, Z.J. 2019. A numerical study on installation effects and long-term shaft resistance of pre-bored piles in clay. *J. Transp. Res. Board* 2673(3), 494–505.
- Li, L., Chen, S.L., Zhang, Z.J., 2020. A practical analytical approach for estimating long-term and setup shaft resistance of pre-bored piles. *J. Geotech. Geoenviron. Eng.* 146(10), 04020100. 1–11.
- Li, L., Li, J.P., Sun, D.A., 2016. Anisotropically elasto-plastic solution to undrained cylindrical cavity expansion in K_0 -consolidated clay. *Comput. Geotech.* 73, 83–90.
- Li, L., Li, J.P., Sun, D.A., Gong, W.B. 2017. Time-dependent bearing capacity of a jacked

- pile: an analytical approach based on effective stress method. *Ocean Eng.* 143(1), 177–185.
- Li, L., Li, J.P., Sun, D.A., Gong, W.B., 2019. A feasible approach for predicting time-dependent bearing performance of displacement piles from CPTu measurements. *Acta Geotech.* 15, 1935–1952.
- Liang, Q., Li, J., Wu, X., Zhou, A., 2016. Anisotropy of Q2 loess in the Baijiapo Tunnel on the Lanyu Railway, China. *Bull. Eng. Geol. Environ.* 75(1), 109–124.
- Mayne, P.W., 1991. Determination of OCR in clays by piezocone tests using cavity expansion and critical state concepts. *Soils Found.* 31(2), 65–76.
- Mo, P.Q., Marshall, A.M., Yu, H.S., 2016. Interpretation of cone penetration test data in layered soils using cavity expansion analysis. *J. Geotech. Geoenviron. Eng.* 143(1), 04016084. 1–10.
- Mo, P.Q., Yu, H.S. 2016. Undrained cavity-contraction analysis for prediction of soil behavior around tunnels. *Int. J. Geomech.* 17(5), 04016121.1–10.
- Mo, P.Q., Yu, H.S. 2018. Drained cavity expansion analysis with a unified state parameter model for clay and sand. *Can. Geotech. J.* 55(7), 1029–1040.
- Randolph, M.F., 2003. Science and empiricism in pile foundation design. *Géotechnique* 53(10), 847–875.
- Randolph, M.F., Carter, J.P., Wroth, C.P., 1979. Driven piles in clay—the effects of installation and subsequent consolidation. *Géotechnique* 29(4), 361–93.
- Rezania, M., Nezhad, M.M., Zanganeh, H., Castro, J., Sivasithamparam, N., 2017.

- Modeling pile setup in natural clay deposit considering soil anisotropy, structure, and creep effects: case study. *Int. J. Geomech.* 17(3), 04016075. 1–13.
- Russell, A.R., Khalili, N. 2006. On the problem of cavity expansion in unsaturated soils. *Computation Mech.* 37(4), 311–330.
- Sivasithamparam, N., Castro, J. 2020. Undrained cylindrical cavity expansion in clays with fabric anisotropy and structure: theoretical solution. *Comput. Geotech.* 120, 103386.
- Sivasithamparam, N., Castro, J., 2018. Undrained expansion of a cylindrical cavity in clays with fabric anisotropy: theoretical solution. *Acta. Geotech.* 13(3), 729–746.
- Su, D. 2020. Drained solution for cylindrical cavity expansion in modified Cam Clay soil under constant vertical stress. *Can. Geotech. J.* doi.org/ 10.1139/cgj-2019-0815.
- Suzuki, Y., Lehane, B., 2015. Analysis of CPT end resistance at variable penetration rates using the spherical cavity expansion method in normally consolidated soils. *Comput. Geotech.* 69, 141–152.
- Vrakas, A., 2016. A rigorous semi-analytical solution for undrained cylindrical cavity expansion in critical state soils. *Int. J. Numer. Anal. Meth. Geomech.* 40(15), 2137–2160.
- Vrakas, A., Anagnostou, G., 2014. A finite strain closed-form solution for the elastoplastic ground response curve in tunnelling. *Int. J. Numer. Anal. Meth. Geomech.* 38(11), 1131–1148.
- Vrakas, A., Anagnostou, G., 2015. A simple equation for obtaining finite strain solutions from small strain analyses of tunnels with very large convergences. *Géotechnique*

65(11), 936–944.

Wroth, C.P., Windle, D., 1975. Analysis of the pressuremeter test allowing for volume change. *Géotechnique* 25(3), 598–604.

Yang, C.Y., Li, J.P., Li, L., Sun, D.A., 2020. Expansion responses of a cylindrical cavity in overconsolidated unsaturated soils: A semi-analytical elastoplastic solution. *Comput. Geotech.* doi.org/10.1016/j.compgeo.2020.103922.

Yu, H.S., 1990. Cavity expansion theory and its application to the analysis of pressuremeters. Ph.D. Thesis. Oxford: St Anne's College, Oxford University.

Yu, H.S., 2000. Cavity expansion methods in geomechanics. Kluwer Academic, Dordrecht.

Yu, H.S., Rowe, R.K., 1999. Plasticity solutions for soil behavior around contracting cavities and tunnels. *Int. J. Numer. Anal. Meth. Geomech.* 23(12), 1245–1279.

Zhao, J.D., 2011. A unified theory for cavity expansion in cohesive-frictional micromorphic media. *Int. J. Solids Struct.* 48(9), 1370–1381.

Zhou, H., Kong, G. Liu, H., 2016. A semi-analytical solution for cylindrical cavity expansion in elastic–perfectly plastic soil under biaxial in situ stress field. *Géotechnique* 66(7), 584–595.

Zhou, H., Kong, G.Q., Liu, H.L., Laloui, L., 2018. Similarity solution for cavity expansion in thermoplastic soil. *Int. J. Numer. Anal. Meth. Geomech.* 42(2), 274–94.

Zhou, X.Y., Xu, Y.S., Sun, D.A., Tan, Y.Z., Xu, Y.F., 2021. Three-dimensional thermal-hydraulic coupled analysis in the nuclear waste repository. *Ann. Nucl. Energ.* 151, 107866.

Zou, J.F., Feng, W., An, W., 2019. A semi-analytical solution for shallow tunnels with radius-iterative-approach in semi-infinite space. *Appl. Math. Model.* 73(9), 285–302.

Table 1. Recent representative solutions to cylindrical cavity expansion

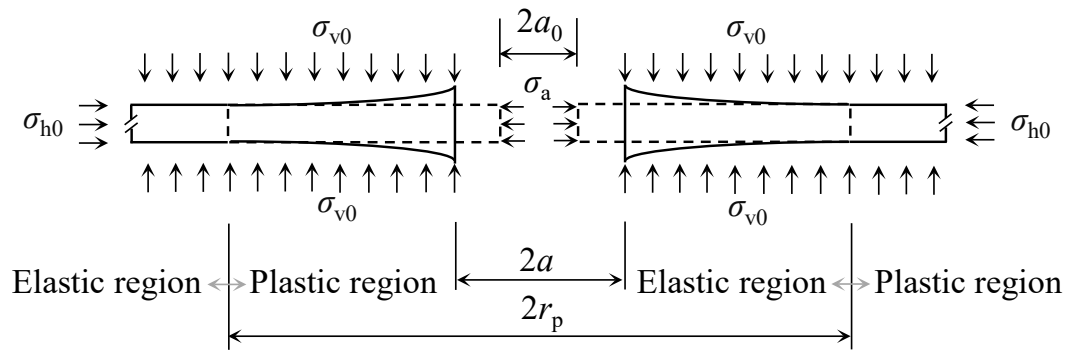
Reference	Model	Hardening Law	Soil Type	Plane Condition
Chen and Abousleiman (2012)	Modified Cam-clay	Volumetric	Isotropic saturated clay	Plane strain
Vrakas (2016a)	Two-invariant critical state models	Volumetric	Isotropic saturated clay	Plane strain
Li et al. (2017)	Anisotropic modified Cam-clay	Volumetric	Isotropic saturated clay	Plane strain
Sivasithamparam and Castro (2018)	S-CLAY1	Volumetric and rotational	Anisotropic saturated clay	Plane strain
Mo and Yu (2018)	Unified state parameter model	Volumetric	Isotropic clay and sand	Plane strain
Chen and Liu (2019)	Dafalias' anisotropic modified Cam-clay model	Volumetric and rotational	Anisotropic saturated clay	Plane strain
Chen et al. (2019)	Anisotropic modified Cam-clay with SMP criterion	Volumetric and rotational	Anisotropic saturated clay	Plane strain
Su et al. (2020)	Modified Cam-clay	Volumetric	Isotropic saturated clay	Plane stress
Chen et al. (2020)	Unsaturated modified Cam-clay	Volumetric	Isotropic unsaturated soil	Plane strain
Yang et al. (2020)	Unsaturated unified hardening model	Volumetric	Overconsolidated unsaturated soil	Plane strain

Table 2. Parameters of SANICLAY involved in parametric analysis

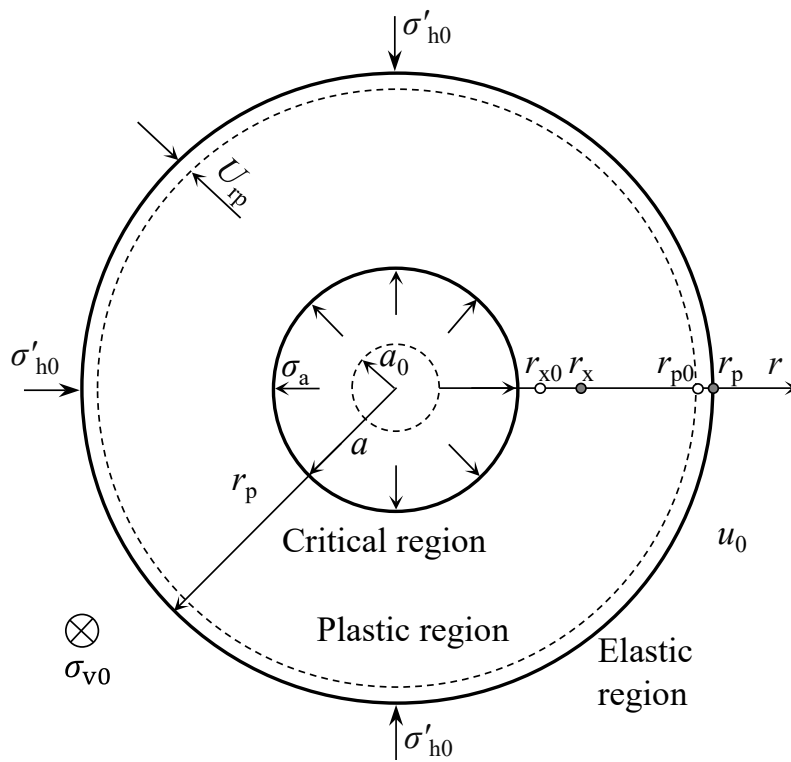
OCR	σ'_{h0} (kPa)	σ'_{v0} (kPa)	u_0 (kPa)	K_0	p'_0 (kPa)	q_0 (kPa)	v_0	G_0 (kPa)
1	100	160	100	0.625	120	60	2.04	20358
5	120	120	100	1	120	0	1.95	19489
7	120	120	100	1	120	0	1.93	19307
10	144	72	100	2	120	72	1.91	19114
20	144	72	100	2	120	72	1.87	18740

$M_c = 1.18, M_e = 0.86, \lambda = 0.063, \kappa = 0.009, \mu = 0.2$

$N = 0.91, x = 1.56, C = 16$



(a)



(b)

Fig. 1. Schematic diagram for undrained expansion of a cylindrical cavity in SANICLAY: (a) front view; (b) plane view

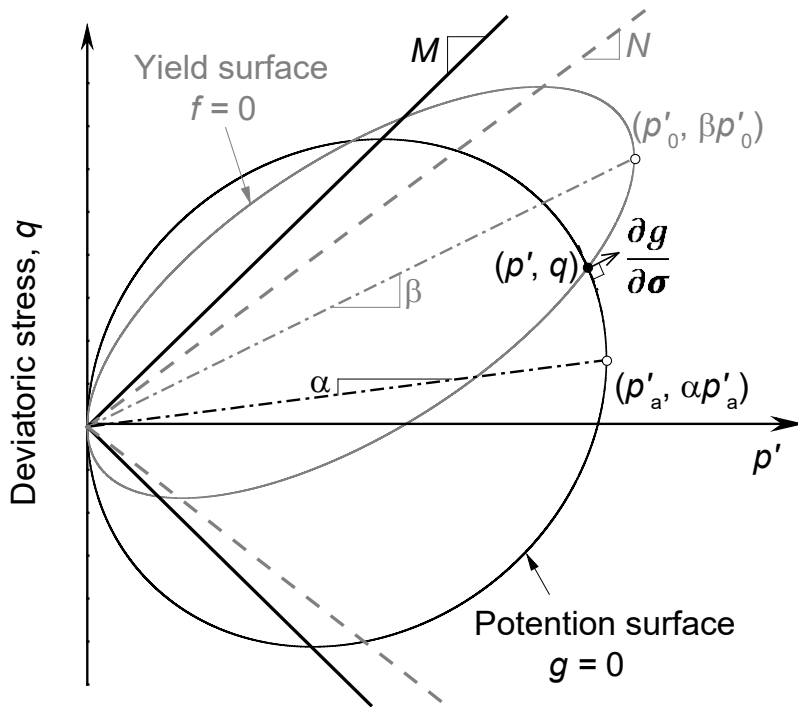
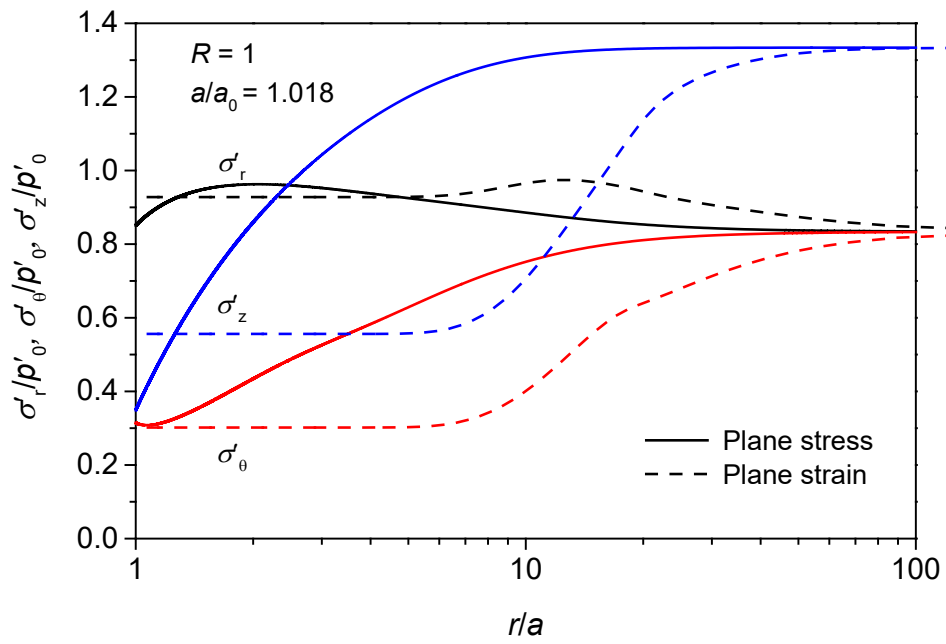
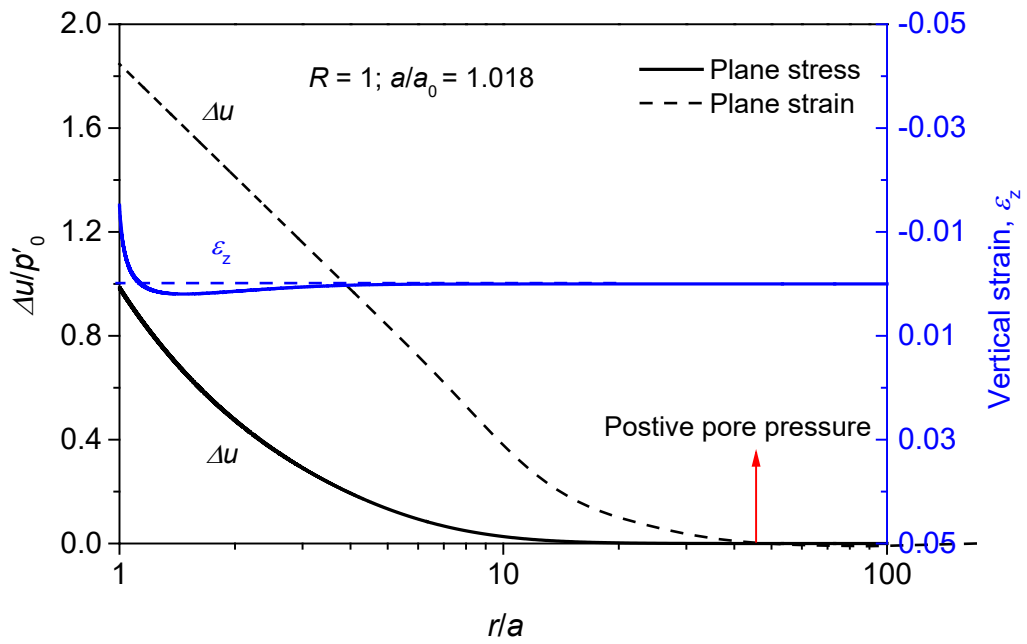


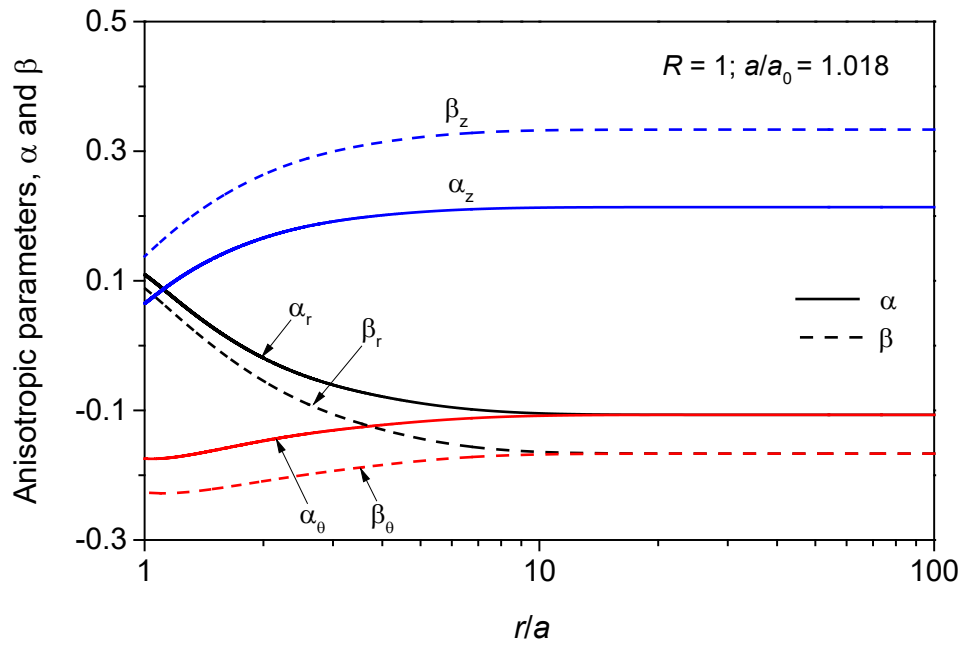
Fig. 2. Yield surface and plastic potential surface of SANICLAY model in $p' - q$ plane



(a)

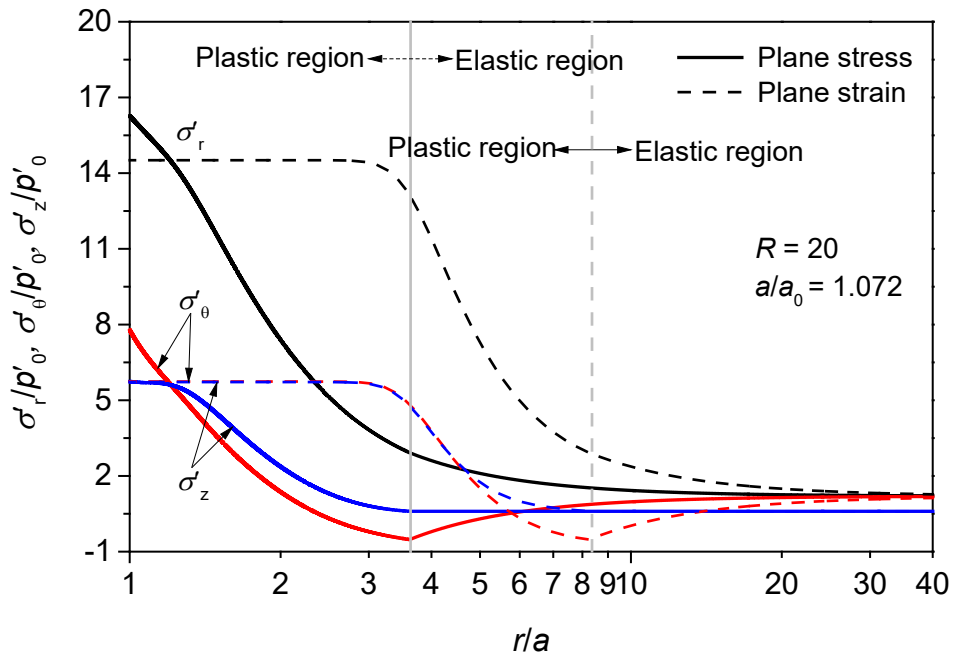


(b)

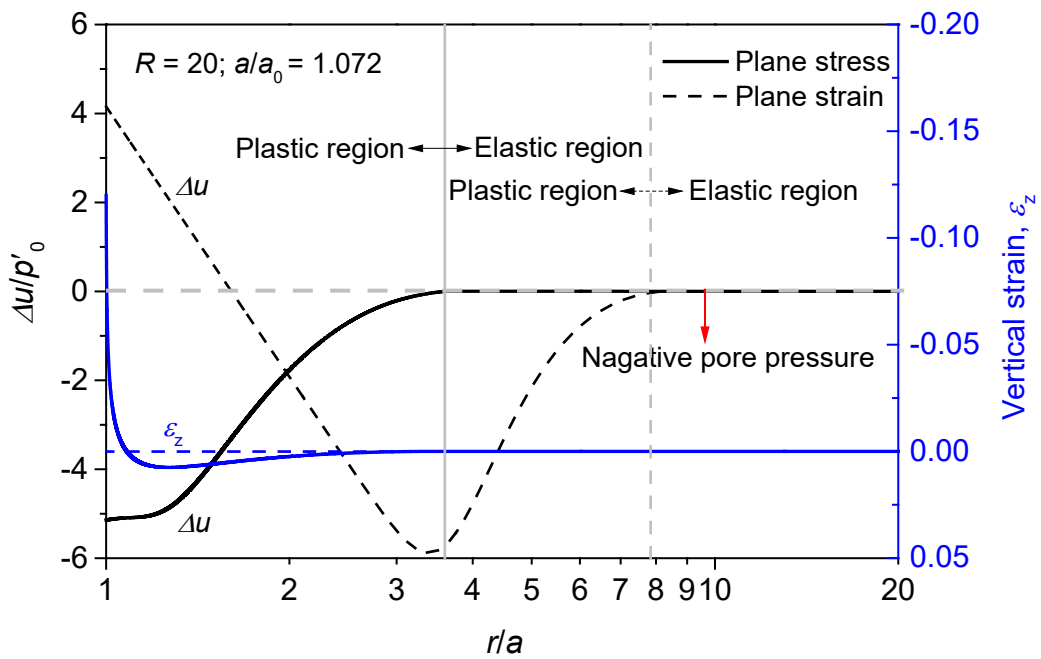


(c)

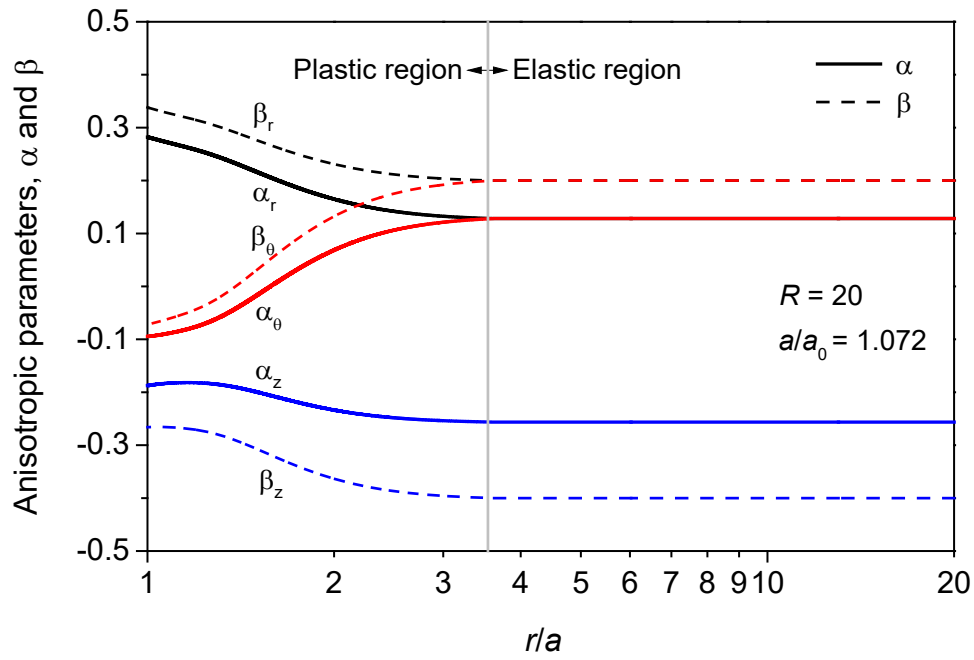
Fig. 3. Distributions of (a) stress components; (b) excess pore water pressure and vertical strain; (c) anisotropic variables around the cavity in normally consolidated soil at instant that soil particle at cavity wall reaches critical state



(a)

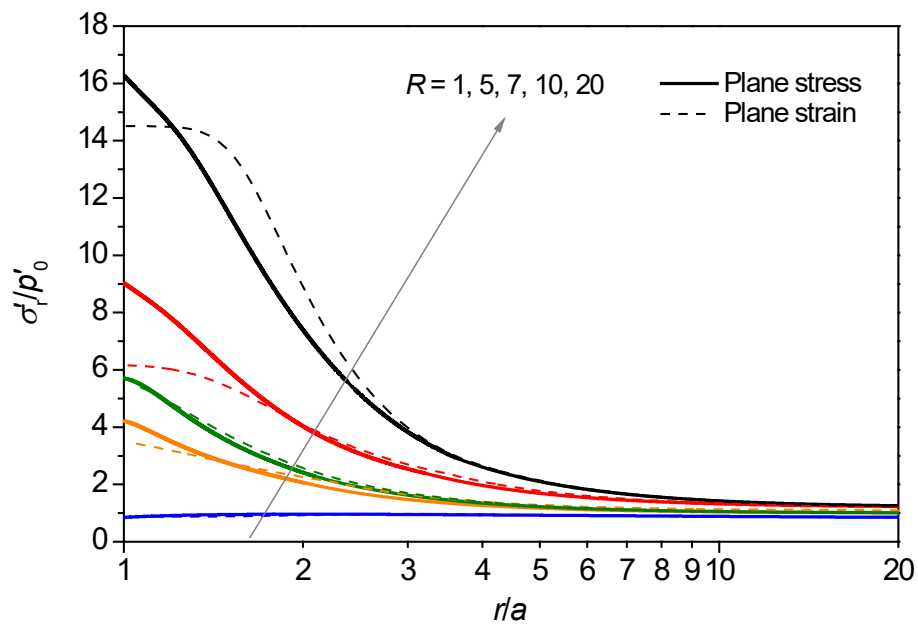


(b)

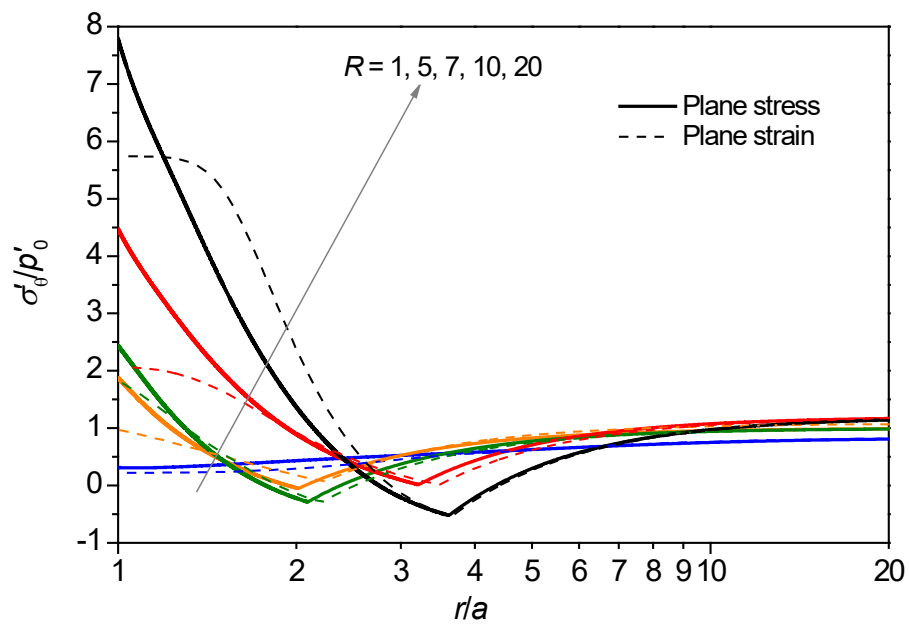


(c)

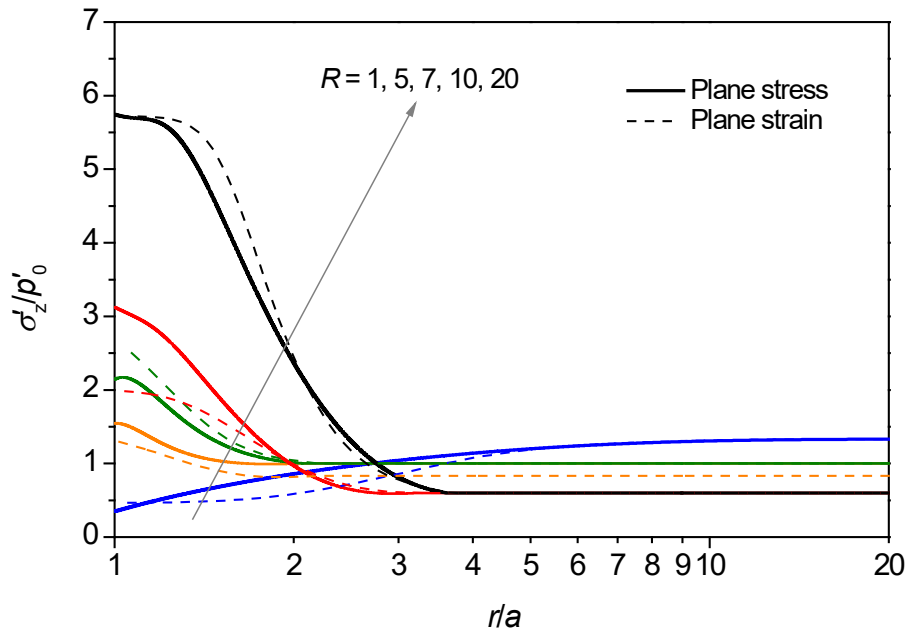
Fig. 4. Distributions of (a) stress components; (b) excess pore water pressure and vertical strain; (c) anisotropic variables around the cavity in heavily overconsolidated soil at instant that soil particle at cavity wall reaches critical state



(a)



(b)



(c)

Fig. 5. Distribution of (a) radial effective stress; (b) tangential effective stress; and (c) vertical effective stress around the cavity at the instant that soil becomes critical state for different overconsolidation ratios

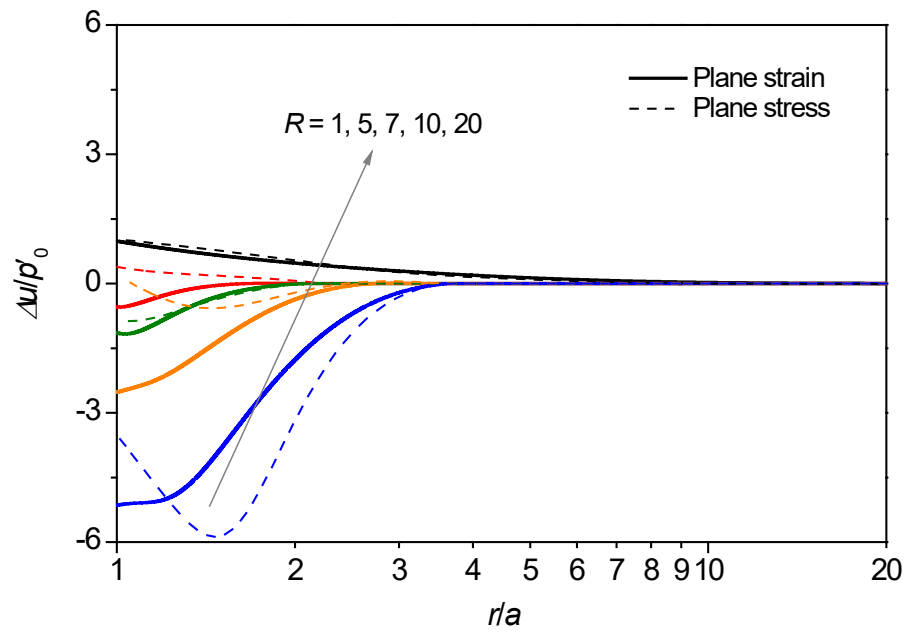


Fig. 6. Distribution of excess pore water pressure around the cavity at the instant that soil becomes critical state for different overconsolidation ratios

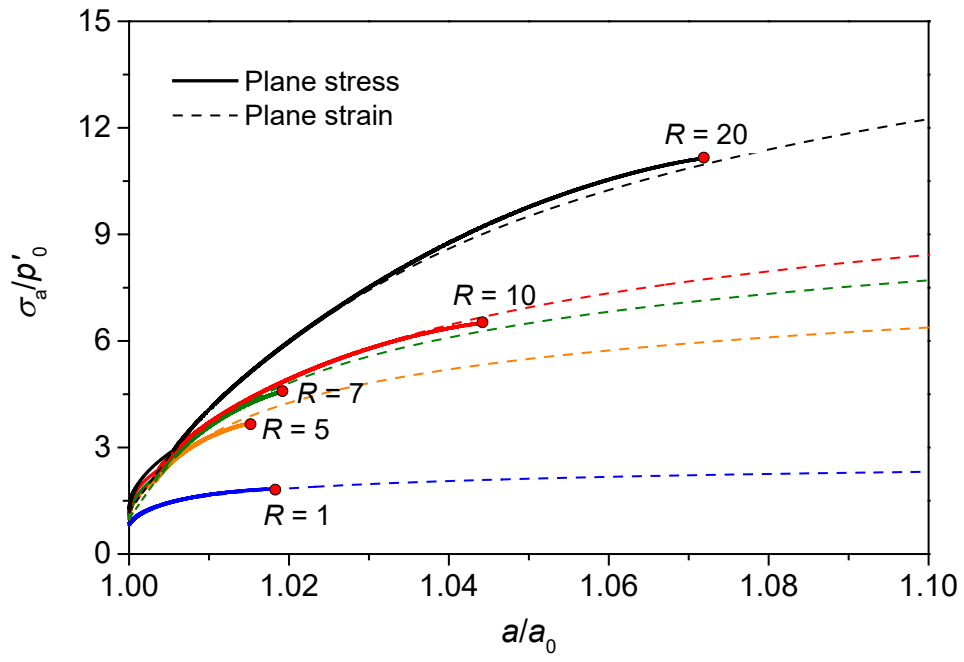


Fig. 7. Expansion-pressure curve during cavity expansion

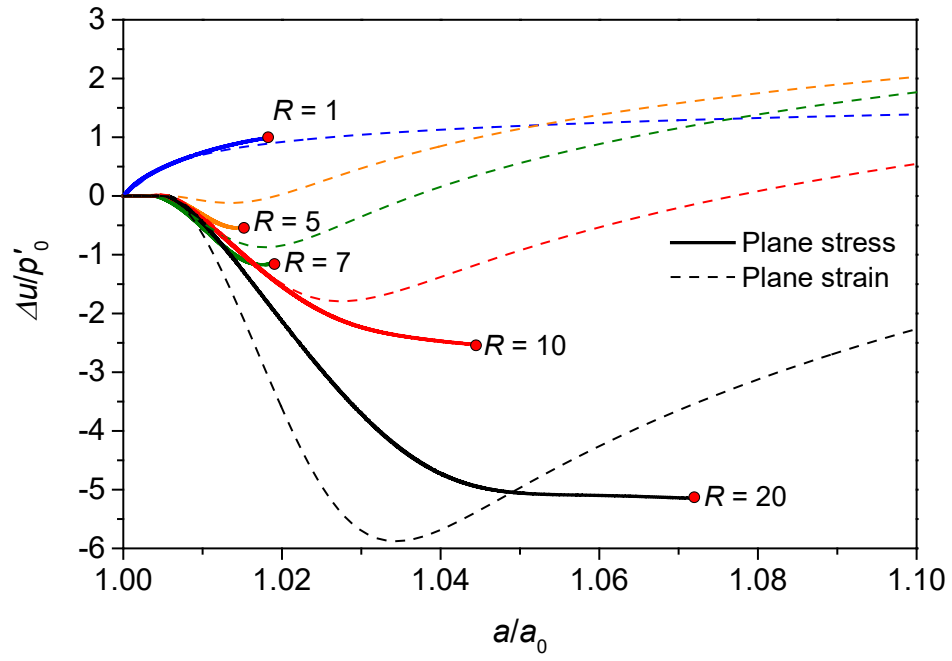


Fig. 8. Excess pore water pressure at cavity wall during cavity expansion

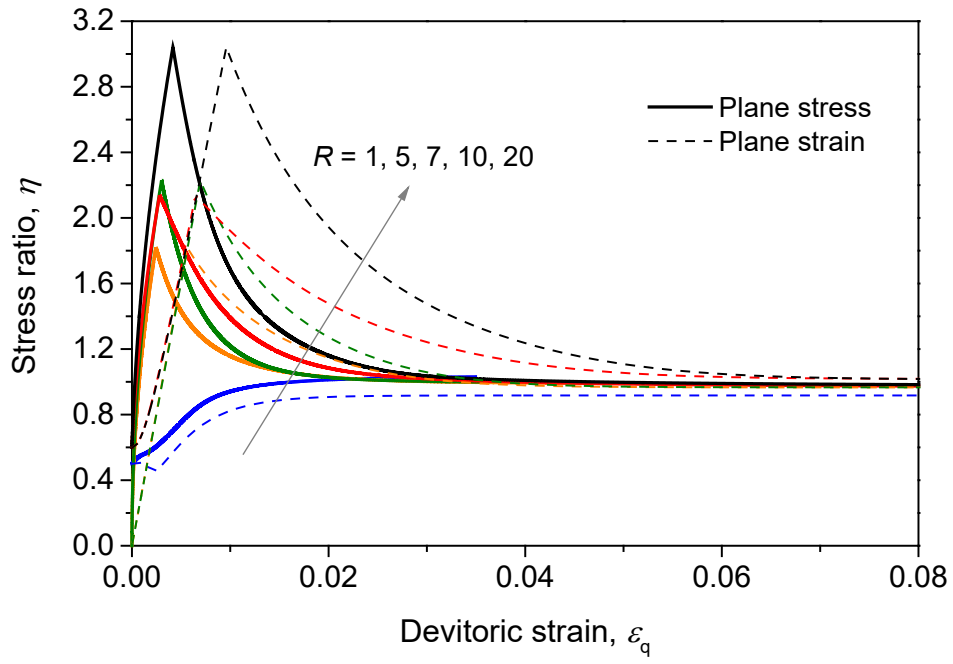
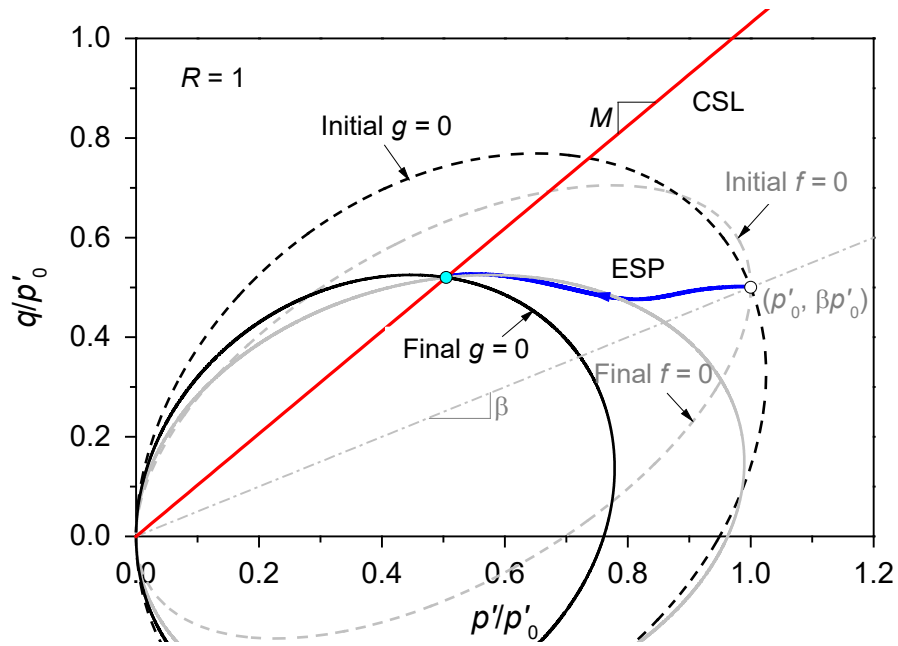
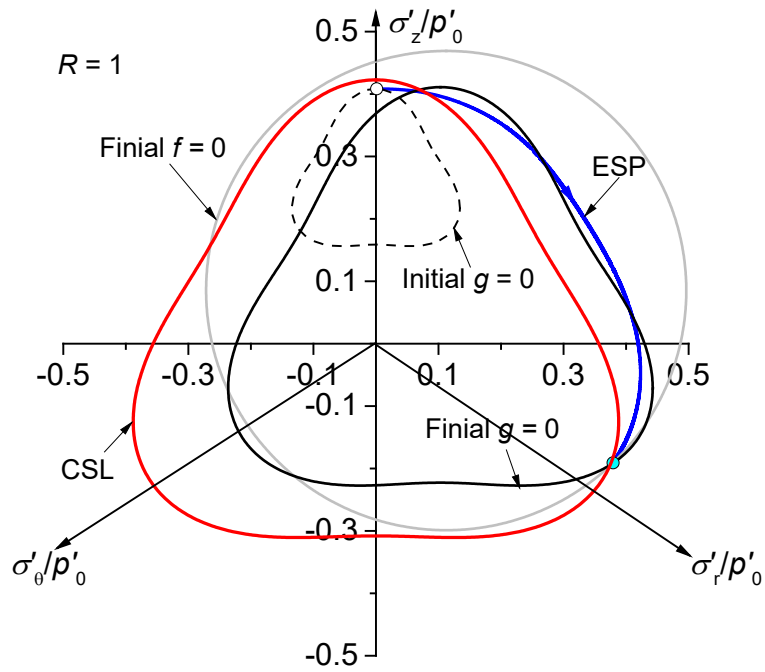


Fig. 9. Variations of stress ratio with deviatoric strain of soil at cavity wall during cavity expansion

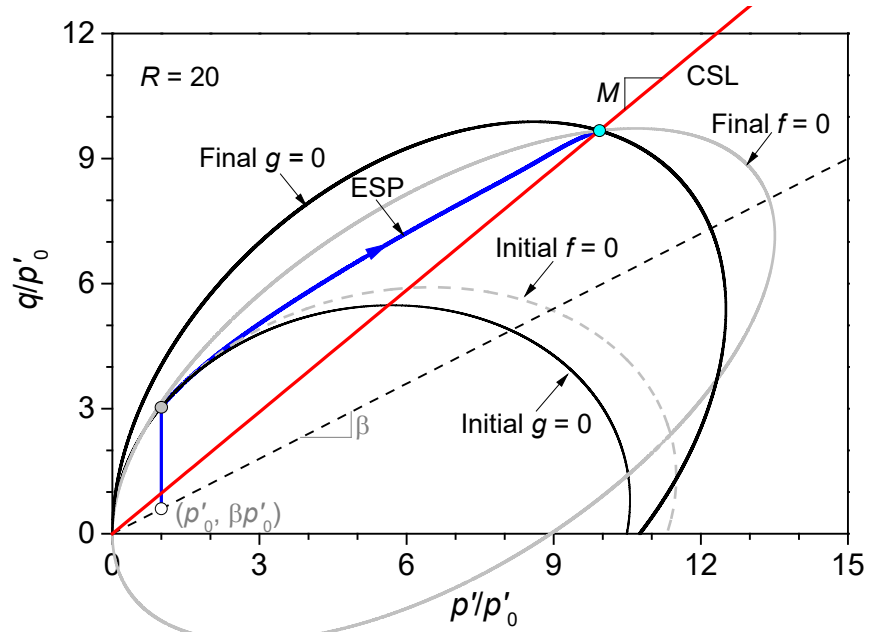


(a)

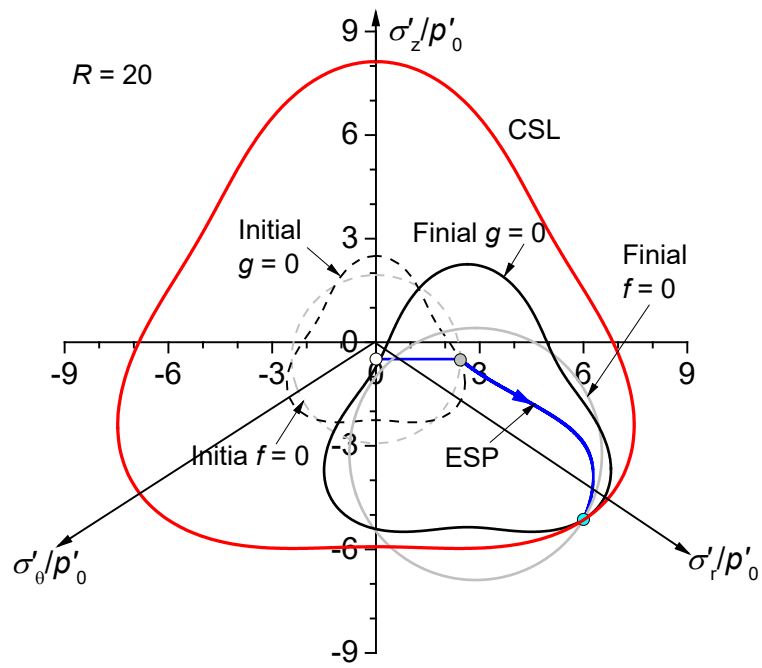


(b)

Fig. 10. Projection of stress trajectory and yield locus in: (a) $p' - q$ plane, (b) π plane
for normally consolidated soil with $R = 1$



(a)



(b)

Fig. 11. Projection of stress trajectory and yield locus in: (a) $p' - q$ plane, (b) π plane
for heavily overconsolidated soil with $R = 20$